

## **Geophysical exploration integrated with hydrogeological data of a deep multiaquifer system: results from a pilot site**

Antonio Bratus, Istituto Nazionale di Oceanografia e Geofisica Sperimentale, Trieste, Italy  
(abratus@ogs.trieste.it)

Dimitra Rapti-Caputo, University of Ferrara, Department of Earth Sciences, via Saragat, 1, I-44100 Ferrara, Italy (cpr@unife.it)

Riccardo de Nardi, University of Ferrara, Department of Earth Sciences, via Saragat, 1, I-44100 Ferrara, Italy (riccardodenardi@libero.it)

Giovanni Santarato, University of Ferrara, Department of Earth Sciences, via Saragat, 1, I-44100 Ferrara, Italy (g.santarato@unife.it)

---

### **SUMMARY**

Fresh groundwater is a strategic resource which is increasingly threatened by human activities. Saving this precious resource demands sound knowledge of the subsurface, of the potential sources of pollution, of the equilibrium between exploitation and recharge processes.

In the present paper a case study is presented where a detailed three-dimensional resistivity model was obtained using Electrical Resistivity Tomography (ERT) and Time-Domain electromagnetic soundings (TDEM). The model not only is in excellent agreement with known geology and hydrogeology, but also shows the presence of a deep, thick layer which could be a huge fresh-water reservoir. Repeated TDEM measurements show resistivity variations in the exploited aquifer which are again in good agreement with direct hydrogeological information.

**Keywords:** Groundwater monitoring, Electrical resistivity Tomography, Time-domain electromagnetic sounding.

---

### **INTRODUCTION**

Groundwater resources of urbanised areas are increasingly threatened by human activities, which can pollute recharge areas or even lead to an overexploitation. Saving these precious resources requires a careful management and legislation. Often the management is subdivided obeying administrative boundaries, while groundwater reservoirs obey to natural boundaries and conditions.

Accordingly, the integrated analysis of hydrogeological, hydrogeochemical and geophysical data allow us to better define the influence of the parameters of the hydrological cycle relative to the qualitative and quantitative characteristics of the aquifer system. As an example of this integrated approach, a test area was selected in northern Italy which is the borehole field of a civil use aqueduct (the "Torrato" field, Figure 1).

### **THE TEST AREA: HYDROGEOLOGICAL OUTLINE**

In the subsurface of the selected test area, one of the most important aquifer systems of Europe is present, which extends from the Friuli to the Lombardy regions all along the pedemountain belt separating the Prealps from the Po River alluvial plain and the Venetian-Friuli plains. This aquifer system, spanning some hundreds km, is known as 'resurgence line' generally occurs as a multi-aquifer system. The system consists of a sequence of several thick alluvial cones characterised by a high hydraulic permeability (Figure 2). Due to the intense farming and industrial activities as well as the intense urbanisation, this multi-aquifer system is characterised by a high vulnerability, both in the exploitation and in the recharge areas.

The hydrogeological conceptual model differs north and south the resurgence or spring line. In the northern

sector, it consists of an unconfined indifferiated aquifer, made up by coarse-grained gravel/sandy material and about 20 to 100 m thick. The main supply for this aquifer body is through vertical infiltration of rainfall and lateral infiltration from the Tagliamento river bed. As a consequence of its high permeability, this aquifer body is very vulnerable to surface pollution.

In contrast, south of the spring line, a multi-aquifer system is present, made up of one unconfined body and, at increasing depths, of several confined aquifer bodies of variable thickness and hydraulic permeability, mainly consisting of sandy/gravel material.

In the test area, which is located south of the resurgence line, the presence of two confined aquifers is known from direct investigation through exploitation drilled down to 300 m below ground level (b.g.l.). The electrical conductivity of the first confined aquifer, whose top is about 30 m b.g.l., presents seasonal variation between 600 and 800 microS/cm, while in the second confined aquifer (180 m b.g.l., 20 m thick) this parameter did not display any significant fluctuations during the hydrological cycle .

## GEOPHYSICAL INVESTIGATION

A geophysical surveys, composed of three-dimensional (3D) reflection seismics and resistivity measurements has been programmed in two different times to get the evolution of the confined aquifers under exploitation, besides the whole knowledge of the buried geology.

In this paper we present the results obtained by the resistivity measurements.

These data were gained by combining Electrical Resistivity Tomography (ERT) to get the best detail of the shallower part (from surface to about 100 m b.g.l.) and Time-Domain ElectroMagnetic soundings (TDEM) to get the whole 3D resistivity model of the subsurface down to the maximum investigation depth of about 1000 m b.g.l. The acquisition parameters of TDEM data were as follows: a)transmitter loop: 200x200 m square loop, b)receiver loop: 100 circular turns of 1 m diameter, c)Geonics TEM57/PROTEM time gates spanning high to medium frequencies (.087 to 28.1 ms). Some cultural noise perturbed the latest time gates. A number of 14 TDEM soundings was executed in the area using 3 transmitter loops and measurement points both inside and outside the loops, at an average distance of 200 m. An area of about 0.5 km<sup>2</sup> was thus investigated.

Occam's style inversion of ERT and TDEM data was performed using commercial software (RES3DINV:

Loke and Barker 1996a, 1996b; EMIGMA: e.g. Parker et al. 1997). The estimated model furnished a detailed map of the resistivity distribution from the surface to the maximum depth of investigation (Figure 3). Based on the hydrogeologic conceptual model and on in-situ measured resistivity values of the bearing water, the model defines with great detail the first confined aquifer, buried between 30 and 60 m b.g.l. As far as the aquifer buried at about 180 m b.g.l. is concerned, its depth to thickness ratio is unfavourable, and therefore it was not well resolved by indirect measurements. Based on regional geologic knowledge of the subsurface at depth, the resistive body, laying at about 350 m b.g.l., and whose thickness was estimated to be at least 200 m, should be composed of coarse, porous sediments and thus it is potentially a huge fresh-water reservoir, not already detected by direct investigation in the test area.

Repeated TDEM measurements after 6 months showed a resistivity variation of about 12-14%, within the first confined aquifer, which resulted in excellent agreement with direct fresh water conductivity measurements. This variation is to be connected with a different exploitation rate due to seasonal variations of the pumping activity for civil uses.

## CONCLUSIONS

A repeated ERT-TDEM survey was performed in a test area to estimate both the resistivity model of the subsurface, its hydrogeological significance and its variation with time. The test area is characterised by hydrogeological conditions of relevant quality and of vulnerability of fresh groundwater resources. High-density resistivity measurements performed with both ERT and TDEM allowed to get the whole sequence of confined fresh-water aquifers in the area and was successful to monitorise the conductivity evolution of the exploited reservoir.

## ACKNOWLEDGEMENTS

This research was carried out with the financial support of the EC, contract LIFE04 ENV/IT/00500.

## REFERENCES

- Loke, M. H., and Barker R. D., 1996a. Rapid least-squares inversion of apparent resistivity pseudo-sections using quasi-Newton method. *Geophysical Prospecting*, 48, 181-152.
- Loke, M. H., and Barker R.D., 1996b. Practical techniques for 3D resistivity surveys and data inversion. *Geophysical Prospecting*, 44, 499-523.
- Parker D.H., Boivin M., Murray I.R., and Groom R.W., 1997. A case study on the application of the EMIGMA modeling package to Crone data over the SOQUEM

Lac Volant Region, Sept-Îles, Quebec. Extended Abstracts, 67th SEG Conference, Dallas, Texas.

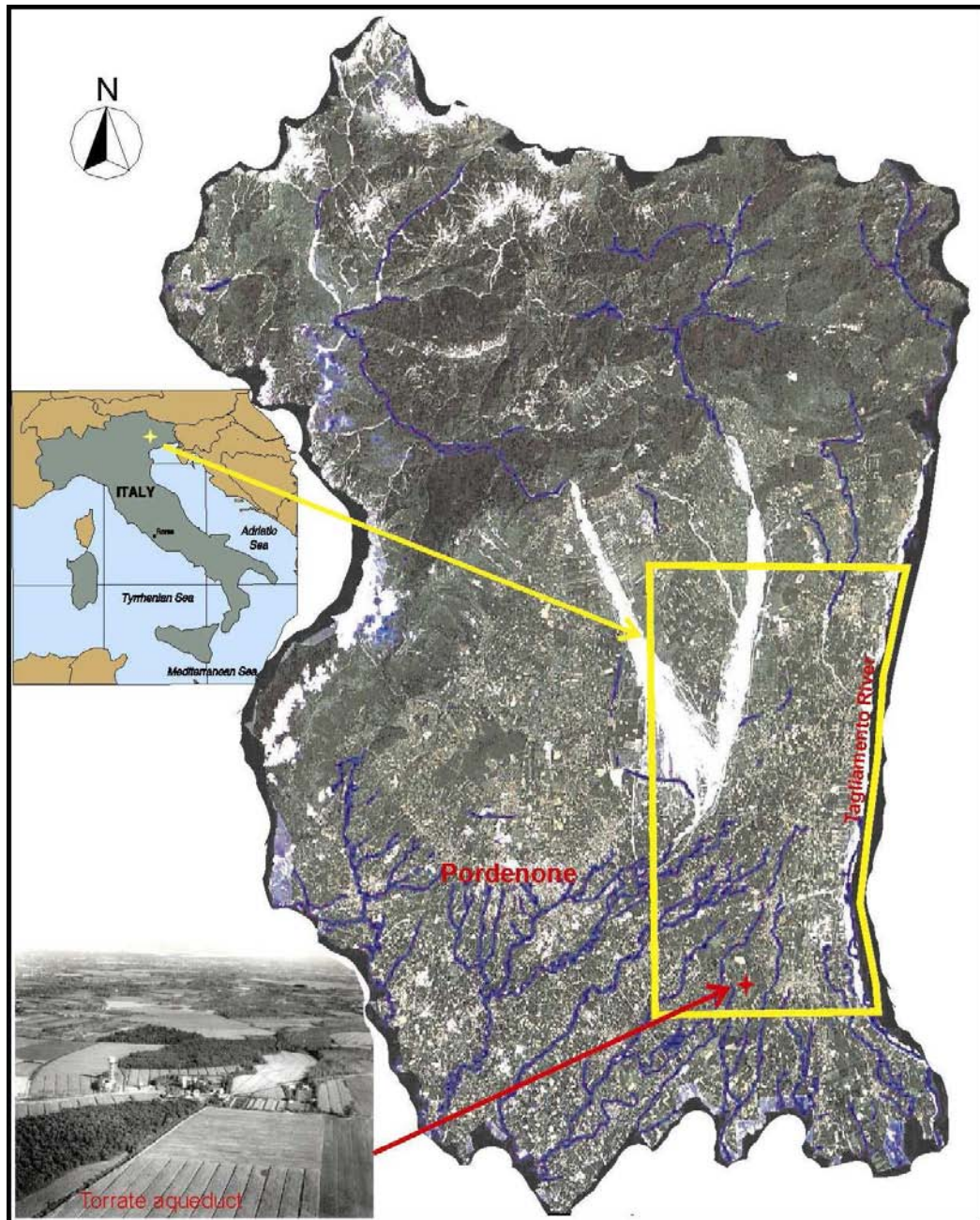


**Figure 1.** The study area

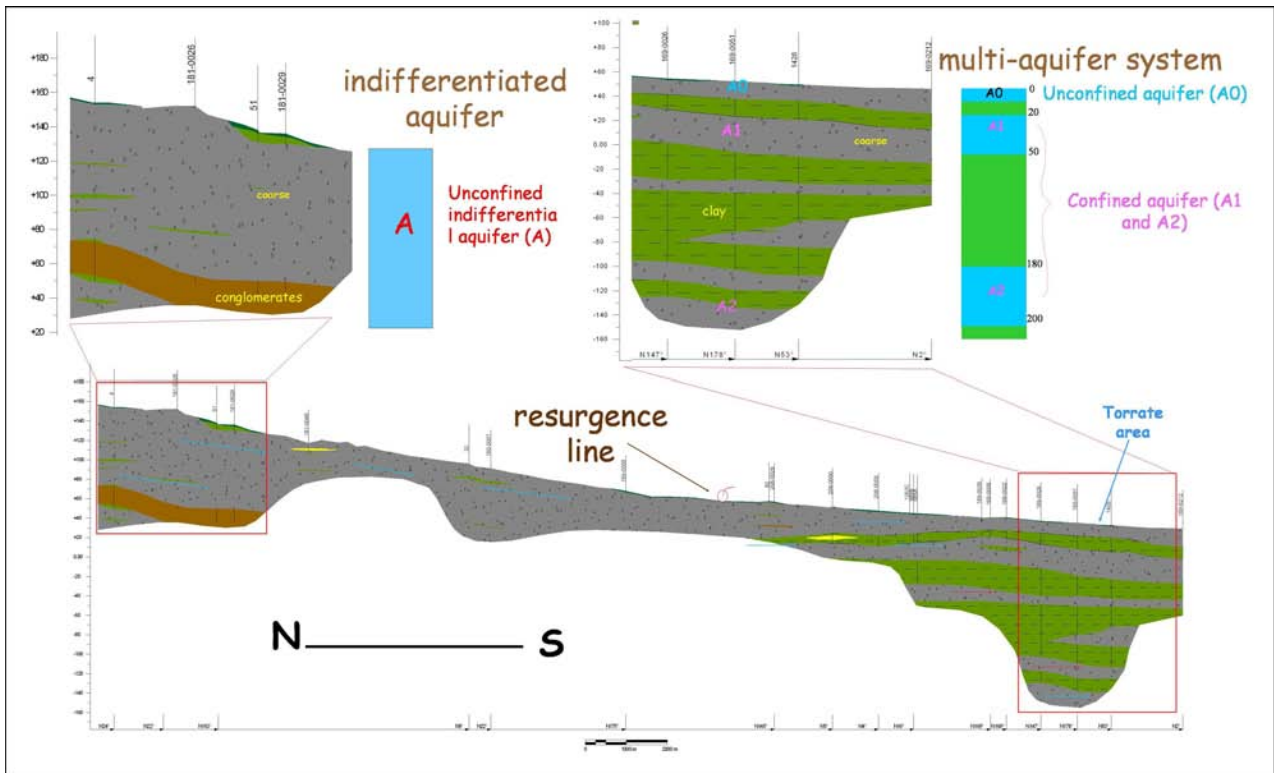


Figure 2. Conceptual hydrogeological model.

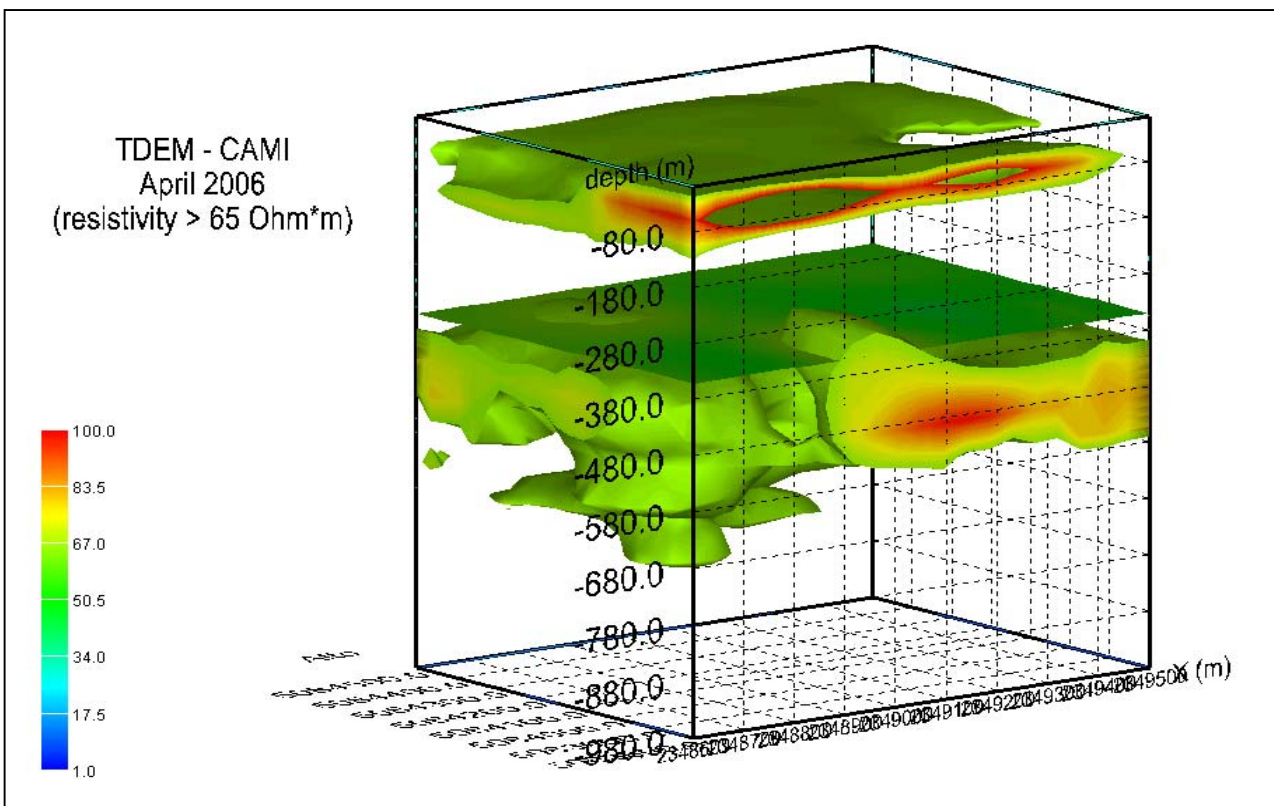


Figure 3. The 3D resistivity model of the test area. For simplicity the volumes with a resistivity greater than 65 Ohm.m have been selected, which contain the most relevant groundwater units of the investigated area.

## AMT and seismic assessment of a Deltaic aquifer system

Ester Falgàs, Universitat de Barcelona, Departament de Geodinàmica i Geofísica, Barcelona, Spain

Juanjo Ledo, Universitat de Barcelona, Departament de Geodinàmica i Geofísica, Barcelona, Spain

Beatriz Benjumea, Institut Geològic de Catalunya, Barcelona, Spain

Alex Marcuello, Universitat de Barcelona, Departament de Geodinàmica i Geofísica, Barcelona, Spain

Pilar Queralt, Universitat de Barcelona, Departament de Geodinàmica i Geofísica, Barcelona, Spain

Teresa Teixidó, Instituto Andaluz de Geofísica, Universidad de Granada, Spain

### SUMMARY

Groundwater research and management requires the understanding of the subsurface properties to constrain multiscale heterogeneities. This work presents a multidisciplinary study focused on the characterization of hydrogeological parameters and processes of a porous aquifer system using geophysical methods sensitive to structures, lithologies, and presence of water, namely Seismic and Audiomagnetotelluric (AMT). The hydrogeophysical experiment is based on the joint interpretation of classical hydrogeological data with seismic profiles and AMT soundings to typify aquifer units, basement depth and state and evolution of the seawater wedge. Tordera deltaic aquifer system is located in the Mediterranean coast of Spain. Forms a small delta of 21 km<sup>2</sup> of detritic unconsolidated materials building up a complex heterogenic aquifer system, confined by Paleozoic granite rocks. Due to tourist and industrial development groundwater resources have incremented its demand during last fifteen years, thus salt-water wedge has progressed inland. Discussion is based on: well lithology descriptions, hydrochemistry, AMT data analysis, seismic tomography models, comparison of 2D AMT inversion models with seismic reflection profiles, and seawater wedge monitoring along the preferential seawater path.

**Keywords:** Audiomagnetotellurics, hydrogeophysics, seawater intrusion

### INTRODUCTION

Tordera delta (Fig.1) is located in the north-eastern coast of Spain. The deltaic aquifer system is built up by quaternary fluvial-deltaic depositional facies above the Paleozoic granitic basement (Geoservei, 2000). Geographically, the deltaic zone is bounded by two main poles of touristy and industrial activities that during last decades have experienced a fast development. Consequently, water demand has increased substantially and seawater wedge has progressed inland reaching some water-supply wells.

Deltaic aquifer systems are complex, and their geological and hydrogeological characterization is a difficult task when only scattered information is available. This work presents a multidisciplinary study focused on the characterization of hydrogeological parameters and processes of the Tordera aquifer system using geophysical methods. We use AMT, seismic reflections and refractions as well as hydrogeological data. Given the different degree of resolution and sensitivity to the presence of water of each method joint interpretation of data will optimize the final models.

### HYDROGEOPHYSICAL SURVEY

Hydrogeophysical data is composed basically from AMT soundings, two seismic lines, and hydrochemical and lithological information (Figure 1).

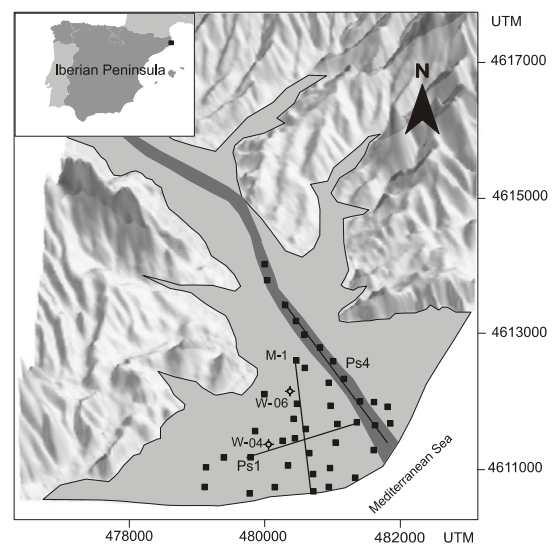


**Figure 1.** Location map of the studied area (vertical scale x10). The position of CSAMT sites are shown by squares, AMT, seismic profiles PS1, PS4 and M-1 by lines, and wells W-06 and W-04.

During spring 2004, 41 AMT sounding distributed over the western deltaic zone were carried out. In addition two more site lines have been performed, 1) on the actual riverbed due to a collocated seismic line, and 2) along the main seawater intrusion path (M-1). The later has been repeated every four month.

AMT survey has been carried out with Stratagem system (Geometrics, 2000) that record in a frequency range form 10 Hz to 92 KHz. High frequency band (>800 Hz) uses an external source to improve the signal to noise ratio in order to fulfill the plain wave assumption, typical distance among transmitter and receiver system in this area has been among 110-200 m.

Seismic data were acquired using 48-channel digital seismograph, 40 Hz geophones and 5 m shot and receiver spacing (Texidó 2000). A roll-along system allows keeping an end-shooting geometry along the profile. Same center spread shots were additional carried out for refraction purposes. Here we present two lines Ps4 along the riverbed with 2400m length and Ps1 parallel to the shore line with 1200 m length.

According to hydrogeological data, we present only two recent multitube piezometers w-06 w-04. Lithological description and three independent hydrochemitry analysis (ACA) at depth (chlorine concentration and electric water conductivity) has been considered in order to compare and to calibrate the geophysical models (Fig.3).

**RESULTS**

AMT data analysis has been done through resistivity pseudo-sections of the impedance tensor determinant at different frequencies. Moreover, dimensionality analysis has also been done with WAL invariants (Weaver, 2000) following the scheme proposed by Martí et al., (2004). Although pseudo-sections and WAL invariants show three-dimensional data behavior dominancy, 2D inverse models were obtained along selected lines as first approximations (Fig.2, 4). Ps1 and Ps4 models (collocated with the seismic lines) fit the apparent resistivity and phases of the impedance tensor determinant, using the algorithm of Siripunvaraporn and Egbert (2000) and following the modifications by Pedersen and Engels (2005).

Main preferential seawater path has been monitored every four month. Electrical resistivity time variation values are expected due to seawater variation conditions. Six models beginning on April 2004 until December 2006 has been performed. Models has also been inverted using the determinant of the impedance tensor, however in those cases we used same layered initial model to emphasize variations only due to seawater content (Fig.4).

Seismic lines PS1 and PS4, has been reprocessed to obtain reflection and refraction models. In these study they has been used both models to constrain basement depth for the AMT collocated models, reducing the inverse equivalence problem.

**DISCUSSION**

Data analysis of the apparent resistivity frequency pseudo-sections show main features of the aquifer deltaic system. Has been well recognized the main seawater intrusion paths over the deltaic space related to an ancient paleochannel oblique to the actual Tordera River, leading the decision of monitoring this specific profile every four month (M-1). Basement presence is also well recorded with AMT data however seismic lines has been used to constrain the depth.

Seismic lines present variable data quality due to variations on the water table, thus to delineate basement depth has been used reflection and refraction models looking for deep reflectors and high velocity values. (Fig.2).

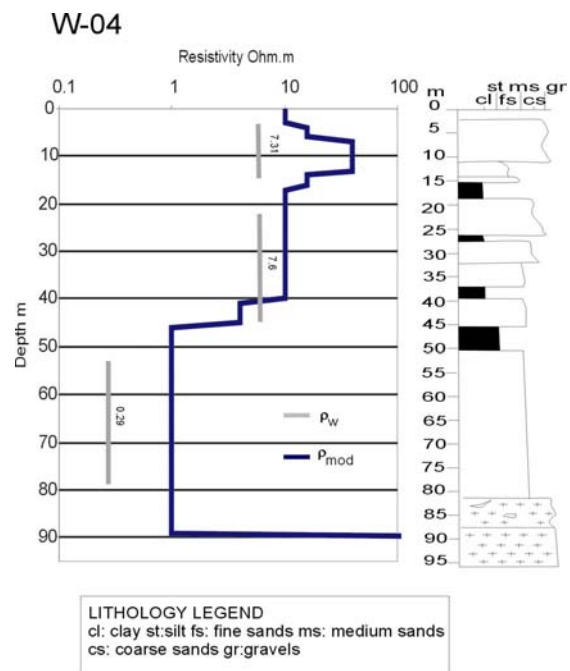


**Figure 3.** Plot diagram of water resistivity ( $\rho_w$ ) and AMT bulk resistivity ( $\rho_{mod}$ ) on wells W-04. Resistivity data is correlated in depth with lithologies.

AMT inverse seismic constrained models have been interpreted using calibration between chlorine concentration, water resistivity and bulk resistivity of the 2D models (Fig.3). Aquifer units carrying fresh water presents high resistivity values ranging from 40 to 1000 Ohm.m, whereas zones of lower hydraulic conductivity (clay interbedded layers) present lower

resistivity from 10 to 40 Ohm.m. Seawater bearing units have been identified clearly on the three AMT profiles PS1, PS4 and M-1, and its AMT estimated resistivity is around 1 to 5 Ohm.m. The chlorine concentration in w-04 and w-06 are 16000 ppm and 1350 ppm respectively around 50 m depth showing the evolution inland of the mixing zone (see location map Fig. 1).

Regarding to the AMT models it is possible to get a preliminary overview of the aquifer system state over the space. Along the riverbed, Ps4 model, seawater intrusion is restricted from 500 m towards the shoreline whereas on the western part of the delta (Ps1 and M1) models seawater intrudes through an ancient paleochannel. Further north in the Ps4, reflects the geoelectrical aquifer structure, relative low resistivity nearsurface zone above high resistive unit related with the main freshwater aquifer unit. Ps1, parallel to the shoreline, presents also this relative low resistive upper zone over a wide an almost continuous low resistive area, related with the intrusion path. And finally, M-1 profile shows the far reaching influence of the seawater wedge and mixing zone.

Monitoring sequence models (Fig.4) from April 2004 to December 2006 show changes on the low resistive layer associated to the seawater wedge. Specifically it can be regarded on the upstream zone of the profile. Figure 4 present only three M-1 models as an example of a regression and progression of the seawater influence. These tendencies are well correlated with the hydrologic state of the aquifer system.

## CONCLUSIONS

Hydrogeophysical studies provide accurate image of the aquifer properties and hydrodynamic processes. Previous hydrogeological and geophysical data has supplied important preliminary information, however joint interpretation of hydrogeological, AMT and seismic models have contributed to get more insight into the system. Velocity tomography model have witnessed distinct thickness of low velocity materials, morphology and depth of the fresh granite basement. Moreover, they help to constrain AMT basement depth.

Distinct hydrofacies can be recognized according to resistivity model values, and specifically on seawater intrusion influence on the aquifer system. Results provide validation for the inversion models linking the material properties and water quality.

Monitoring profile has tested AMT as a sensitive method to monitor changes in fluid electrical resistivity. Sequence models show the dynamic of the seawater mixing zone as a expression of the hydrologic state of the system.

## ACKNOWLEDGEMENTS

This work was supported by research grant REN2002-04538-C02-01 of the Educational Ministry of Spain. The authors would like to thanks Anna Martí for her help using WAL invariants.

## REFERENCES

- ACA Salinity net control. On line at: [http://mediambient.gencat.newt/aca/ca//medi/aigues\\_suterranies/](http://mediambient.gencat.newt/aca/ca//medi/aigues_suterranies/)
- Geometrics, 2000. Operation Manual for Stratagem systems running IMAGEM. Ver.2.16.
- Geoservei, 2000. Actualització i cartografia hidrogeològica del sistema fluvio-deltaic del curs mitjà i baix del riu Tordera. Informe intern ACA. Barcelona. (Internal).
- Martí, A., P. Queralt, and E. Roca, 2004. Geoelectric dimensionality in complex geological areas: application to the Spanish Betic Chain, *Geophysical Journal International*, 157, 961-974.
- Teixidó, T., 2000. Caracterització del subsòl mitjançant sísmica de reflexió d'alta resolució. Doctoral Thesis, Universitat de Barcelona.
- Pedersen L. B., and M. Engels 2005b. Routine 2D inversion of magnetotelluric data using the determinant of the impedance tensor, *Geophys.*, doi:10.1190/1.1897032.
- Siripunvaraporn, W., and G. Egbert, 2000. An efficient data-subspace inversion method for 2-D magnetotelluric data. *Geophysics*, 65; 3, 791-803.
- Unsworth, M.J., X. Lu, M.D. Watts, 2000. CSAMT exploration at Sellafield: Characterization of a potential radioactive waste disposal site: *Geophysics*, 65, 1070-1079.
- Weaver, J.T., A.K. Agarwal, and F.E.M. Lilley, 2000. Characterisation of the magnetotelluric tensor in terms of its invariants, *Geophys. J. Int.*, 141, 321-336.

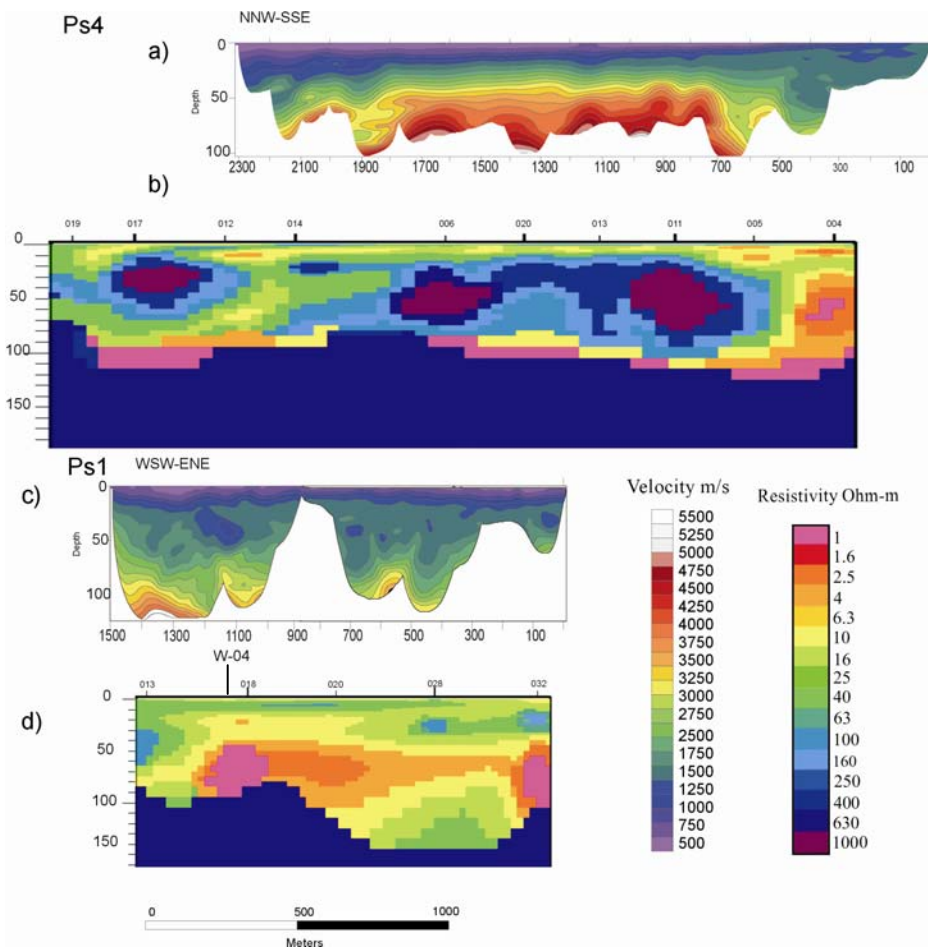


**Figure 2.** AMT and seismic velocity tomography collocated profiles (PS1, PS4), see figure 1 for location. All models are in the same length scale a) PS4 seismic velocity tomography, b) PS4 CSAMT model, c) PS1 seismic velocity tomography, and d) PS1 CSAMT model.

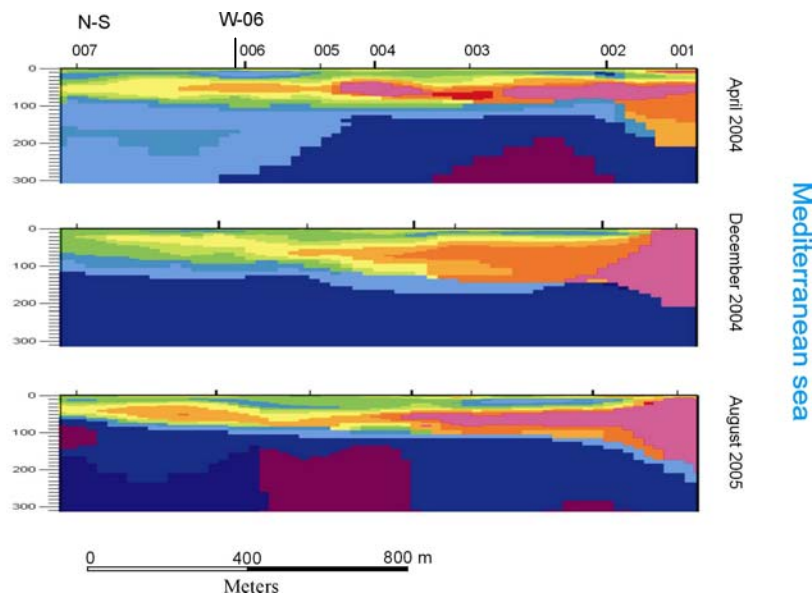


**Figure 4.** Time-lapse AMT modelling. Northern part of the models shows variations on the deep resistivity layer, associated to changes in water salinity content. Resistivity colour-scale same as in figure 2.

## Detecting areas with sulfidic sediments using RMT surveys

Mehrdad Bastani, Lena Persson, and Gustav Sohlenius, Geological Survey of Sweden, Box 670, SE-75128, Uppsala, Sweden

---

### SUMMARY

Sulfidic postglacial sediments occur below the highest coastline in both Finland and Sweden. The sediments were mainly deposited in the Litorina Sea from about 7000 to 4000 years ago. Acid sulfate soils are formed after oxidation of the iron sulphides (e.g. FeS, FeS<sub>2</sub>) in these sediments. High concentrations of certain trace elements (e.g. Ni, Cu and Mn) have been measured in streams, which drains areas dominated by acid sulfate soils (Åström & Björklund, 1995). These trace elements can cause environmental problems.

Studies from such areas in Finland have shown that sulfidic sediments have lower electrical resistivity compared to other fine-grained sediments. The aim of the present work was to find geophysical methods that can be used to identify areas in Sweden where acid sulfate soils and sulfidic sediments occur. We have used different resistivity methods to map the occurrences of the sulfidic sediments in three areas in Sweden. The Radiomagnetotelluric (RMT) in the frequency range 10-250 kHz was used in all three areas and some other electrical resistivity methods were employed to compare the resulting models.

The results show that the RMT method is a powerful tool to use to detect the sulfidic sediments. The results confirmed those reported in Finland (Puranen, et al., 1999) meaning that the sulfidic sediments have generally lower electrical resistivity than the surrounding postglacial sediments (2-100 times lower). The modeled resistivities of the sulfidic sediments have a range of variations and change from one area to another depending on the host sediments. Direct resistivity measurements using a resistivity probe revealed a very good correlation between the measured and estimated resistivities and depths in the Lake Mälaren area.

**Keywords:** Electrical resistivity, Sulfidic sediments, RMT

---

### INTRODUCTION

Acid sulfate soils are formed on sulfidic sediments along the Baltic Sea coast and around Lake Mälaren in Sweden. Oxidation of iron sulfides causes a low pH in these soils. In many areas sulfidic sediments are oxidized due to ditching or construction work (Sohlenius & Öborn, 2004; Lax & Selinus, 2005). High concentrations of certain trace elements (e.g. Ni, Cu and Mn) have been observed in streams draining areas dominated by acid sulfate soils. The trace element contents are not higher in sulfidic clay sediments than in clays, which lack iron sulfides. There is, however, an intense leaching of e.g. Cd and Ni from acid sulfate soils compared to soils formed in clay sediments with no iron sulfides.

Most sulfidic sediments in Sweden have been deposited in brackish water on the floor of the Baltic Sea. The sulfides in the sediments were formed in an anoxic environment some cm below the oxic sediment-

water interface. Along the coast of northernmost Sweden sulfidic sediments underlie a large proportion of arable land. Pyrite (FeS<sub>2</sub>) is the most common sulfide mineral. The sulfidic sediments in northern Sweden have, however, high contents of FeS giving them a characteristic black color. The sulfidic sediments around Lake Mälaren are often characterized by a high FeS<sub>2</sub> and low FeS content. These sediments are found in the lowest topographical areas.

The most important factor, which causes mobilization of trace elements from acid sulfate soils, is increased weathering due to low pH. Nickel, Co, Mn, Mo and Cu are, however, partly bound in pyrite and are mobilized after oxidation of that mineral. The acid sulfate soils are often characterized by vertical iron oxide coated cracks, which can be followed down to the ground water table. The mobilized elements are rapidly transported down through these cracks. At the ground water table these elements are enriched and can be mobilized to the drainage water during heavy rainfall

or snow melt. Cd, Ni, Mn, Co, Zn and to some extent Cu are mobilized from acid sulfate soils whereas Cr and Fe are only mobilized to a limited extent. Cu, Mo and Fe are partly bound in the oxides, which are formed in acid sulfate soils. That decreases the mobility of these elements.

Data from geophysical, biogeochemical and quaternary maps can be used to define the geographical distribution of acid sulfate soils and sulfidic sediments.

Based on the existing information (maps, field observations, etc.) three areas with occurrence of sulfidic sediments were selected (Figure 1).



Figure 1. Location of study areas in Sweden.

The airborne VLF data are used to select the areas contaminated by the sulfidic sediments. The Geological Survey of Sweden (SGU) acquires airborne VLF data along flight lines with a maximum separation of 200 meters and a sampling interval of 15-40 m at a height of about 30-60 m. SGU operates a unique tensor-VLF device in its airborne surveying program since 1995. The 3 components of magnetic field from two different VLF transmitters are measured simultaneously. With this method a response can be calculated that is independent of the transmitter direction (Pedersen et al., 1994). We have used a new method that provides a direct transformation from VLF data into apparent resistivity and phase (Becken & Pedersen, 2003). The resistivity maps obtained in the Lake Mälaren area were primarily used to locate regional areas with clay and possible sulfidic sediments. A significant correlation was found between the clay deposits and the low resistive areas (Persson et al., 2004). The

lowest resistivity areas were covered with gyttja sediments, i.e. clay sediments that contain organic material and often iron sulfides.

In area 1 and 3 at least two methods were chosen to study the sulfidic clays in detail and in area 2 we only used the RMT method.

## GROUND GEOPHYSICAL MEASUREMENTS

In all three areas the RMT method was employed to map the resistivity variations. The instrument used was EnviroMT from Uppsala University (Bastani 2001). The RMT data were collected at stations with 10 m spacing. A 12-dB S/N ratio threshold for the total horizontal magnetic field power was set to select the peaks related to the transmitters. Depending on the locations, the signal from 12 to 24 transmitters were utilized for the data processing.

In area 1 a capacitive system the so-called OhmMapper was also used to collect data along 5 profiles. In addition electrical resistivity was measured with a logging device (*resistivity probe*) on several locations along the profiles (Puranen et al., 1997). In addition to the geophysical measurements, samples from the sediments were taken and later analyzed for the total sulfur content at two locations along the profile. In area 2, close to the city of Umeå, six RMT profiles were measured in 3 different locations. In area 3, close to the city of Luleå, data were also collected along 2 profiles using the multi-electrode Lund system from ABEM AB. The methods used are briefly explained below.

### *EnviroMT (RMT)*

EnviroMT utilizes the electromagnetic signal in the frequency band 10-250 kHz. The sources are powerful VLF and radio transmitters. The collected data are the horizontal electric field components ( $E_x$ ,  $E_y$ ), the horizontal magnetic field components ( $H_x$ ,  $H_y$ ), and the vertical magnetic field components ( $H_z$ ).

### *OhmMapper*

The capacitive measuring system OhmMapper is a high productivity, electrical resistivity mapping system. Because the instrument's transmitter and receiver are capacitively coupled to the ground there is no need for metal probes. The instrument employs the well-known dipole-dipole configuration. A thin transmitting wire, electrified with a 17 kHz signal, is dragged along the ground, inducing current flow in the earth. A matched receiver, tuned to the transmitter frequency, measures the associated voltage. The penetration depth is a

function of the ground resistivity, the dipole length and the receiver-transmitter separation. The capacitive measurements were conducted continuously with a 4 Hz trigger frequency along the profile and the data were registered every 25 cm. The dataset contains measurements with four different dipole lengths of 2.5, 5, 10 and 20m.

#### Multi-electrode system

The instrument used is the Lund imaging system from ABEM AB. A set of steel electrodes is first set up along the desired direction and with a pre-defined sampling interval. The electrodes are then connected to the central processing unit via specific cables. The data acquisition is carried out and controlled by the central unit. The electrode spacing used in this study was a minimum of  $a=5$  m up to  $a=100$  m with a Wenner configuration.

#### Resistivity probe

In addition to the ground measurements a logging device for detailed mapping of electrical resistivity in soft sediments were used at some locations along the profiles. The equipment is constructed by the Geological Survey of Finland (GTK) and consists of a small probe attached to an add-on shaft (Puranen et al., 1997). The sensor is composed of four small steel electrodes (Wenner configuration) fixed into the probe 1.5 cm apart.

## RESULTS

The RMT data are inverted using the REBOCC program by Siripunvaraporn and Egbert 2000. The RES2DINV program is used to invert the OhmMapper and multi-electrode data (Griffiths et al., 1990; Griffiths and Barker, 1993). In area 1 (Lake Mälaren) three profiles in two locations were measured using EnviroMT and OhmMapper. Figure 2 shows the OhmMapper (at the top) and the EnviroMT (at the bottom) resistivity models. A very strong correlation exists between the two models. The OhmMapper model has a better resolution at the top and this is due to the finer sampling along the profile (25 cm between the measuring points). Because of a deeper penetration depth of the RMT signal, the EnviroMT model resolves the features down to a depth of about 30 meters while the OhmMapper model is limited to a maximum depth of 8 meters. Both models show a strong low resistivity anomaly (below  $5 \Omega.m$ ) that starts at the beginning of the profile and continues to 300 m distance. The estimated depths and resistivities in both models are in very good agreement. In order to assess the accuracy of the models, the resistivity of the ground was directly measured in situ from the surface down to a depth of 10 m with a sampling interval of 25 cm at two location along the profile (A and B in figure 2). The measured resistivities versus depths are shown in figure 3. At point A the resistivity drops below  $10 \Omega.m$  at 2 m

depth and reaches a minimum of  $3 \Omega.m$  and rises again at a depth of about 9 m. At location B the resistivity shows the same trend with a more resistive and thinner low resistivity feature. These measurements are perfectly supporting the resistivity-depth models. The soil samples taken from the same locations (A,B) show that the sulfur content are 1.1% and 0.03% at locations A and B, respectively, indicating that the sulfidic sediments has more concentrations at the beginning of the profile.

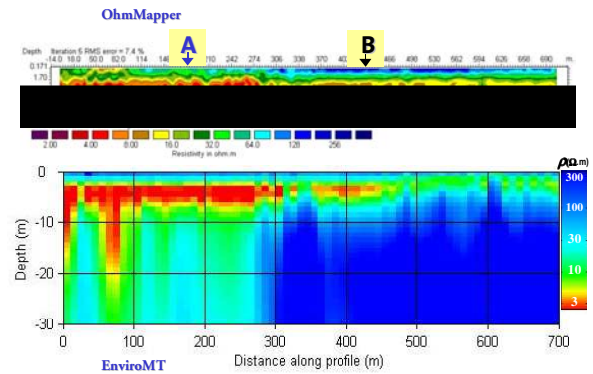


Figure 2. Resistivity-depth models along profile 1 in Fiholm. The OhmMapper model is at the top and the EnviroMT model at the bottom.

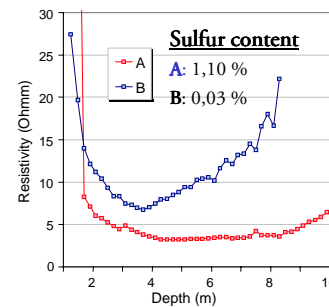


Figure 3. Resistivity-depth variations at locations A and B along profile 1 in Fiholm. The sulphur content measured at these locations shows higher concentration at the beginning of the profile.

The EnviroMT was used in the second area close the town of Umeå to measure the electrical resistivity in three locations. In figure 4 we show the model from the 2D inversion of the RMT data along profile 1 in Umeå. The sulfidic sediments have higher resistivities than those in the Lake Mälaren area. The difference may partly be due to the change in the host sediments and partly due to the lower sodium chloride concentration in the sediments. The sulfidic silts have a significant lower resistivity than the overlying sands.



## Evolution and Distribution of Biogenic Gasses in Peat Soils

Xavier Comas, Rutgers University, Department of Earth and Environmental Sciences, Newark, NJ  
Lee Slater, Rutgers University, Department of Earth and Environmental Sciences, Newark, NJ

---

### SUMMARY

Peatlands are capable to generate significant amounts of free-phase biogenic gases (e.g. methane and carbon dioxide), but considerable uncertainty still exists regarding the mechanisms of formation and spatial distribution of these gasses within the soil matrix. Significant amounts of biogenic gases are released to the atmosphere after formation, but its effect on global warming is still a major uncertainty in climate modeling due to the high temporal and spatial variability in emission rates. In this work we investigate the utility of ground penetrating radar (GPR), to non-invasively image the evolution, spatial location and emission patterns of biogenic gasses in a peat block. A large block (0.022 m<sup>3</sup>) was extracted from a large freshwater peatland in Maine. EM measurements were made as temperature was increased from 5°C until 21°C was reached and held constant. The block was constructed to permit high-frequency GPR measurements (1.2 GHz frequency). Methane emissions and surface peat deformation were monitored concurrently by using a portable methane detector and elevation rods respectively. The results demonstrate that: 1) GPR is a highly effective tool for non-invasive monitoring gas dynamics and spatial distribution within a peat block without disturbing the gas regime; 2) our findings are consistent with previous studies based on gas dynamics in peat soils (including gas volumes, fluxes and thresholds to initiate ebullition); 3) ebullition under our experimental conditions seems to preferentially occur from the near-surface peat; 4) ebullition events seem to exhibit certain periodicity on gas emission, suggesting it may be predictable and therefore could be incorporated into global climate models.

**Keywords:** Peatlands, Biogenic Gas, Ebullition, GPR

---

### INTRODUCTION

Peatlands (or high-latitude wetlands) store about 27% of the global soil carbon and account for approximately 7% of the global annual methane emissions [Khalil, 2000]. CH<sub>4</sub> producing bacteria in the deeper parts of the bog are postulated to generate a reservoir of free-phase methane [Romanowicz *et al.*, 1995] that can be up to three times larger than the reservoir of dissolved phase [Fechner-Levy and Hemond, 1996]. Recent studies investigate the effects of entrapped biogenic gas on peatland hydrology [Beckwith and Baird, 2001; Baird and Waldron, 2003; Kellner *et al.*, 2005], gas emissions and pore water chemistry [Strack *et al.*, 2005]. However, the dynamics (e.g. build-up and evolution) and spatial distribution of entrapped biogenic gasses in peat soils remain uncertain.

Volumetric gas content within the peat matrix has been estimated both at the field and laboratory scale using a range of different techniques. Measurements of free

phase gas (FPG) volume vary depending on location (e.g. 9-13%, Rosenberry *et al.*, 2003; 15%, Kellner *et al.*, 2005; 5-16%, Beckwith and Baird, 2001; or up to 19%, Tokida *et al.*, 2005b), demonstrating the heterogeneous nature of peat soils.

CH<sub>4</sub> emission to the atmosphere occurs by diffusion, wicking through vascular plants, and ebullition (bubbling out) events that can release large volumes of gas over a short time scale [Glaser *et al.*, 2004]. In deeper parts of peat bogs large volumes of FPG may accumulate in bands of relatively inelastic woody peat beneath confining layers that occasionally rupture and bring gas to the surface [Romanowicz *et al.*, 1995; Glaser *et al.*, 2004]. However, ebullition from shallower peat (less than 1 m), where confining layers may be lacking, also occurs [Baird *et al.*, 2004; Strack *et al.*, 2005; Tokida *et al.*, 2005a].

Few studies consider whether emission patterns exhibit any periodicity (and thus might be predictable) or whether they are entirely random in time (Whalen and

Reeburgh, 1992; Glaser *et al.*, 2004). Nonetheless they concluded that the nature of these episodic releases is discontinuous both in time and space, and reiterated the need for wider spatial and temporal scales on ebullition measurements.

Previous studies to estimate the volume of free phase gas in peat involve either (1) destructive/invasive sampling methodologies that potentially disrupt the in situ gas distribution (e.g. insertion of moisture probes, time domain reflectometry (TDR) sensors or elevation rods), or (2) surface-based measurements (e.g. gas chambers, surface deformation) that provide little/no information on the spatial distribution of gasses in the peat soil (see [Comas *et al.*, 2005] for review). We report here EM measurements, supported by surface elevation rod measurements and gas fluxes estimated with a portable methane detector as a completely non-invasive approach for investigating gas dynamics in peat blocks. Our EM results yield insights into the temporal build up of free phase gas, the spatial distribution of free phase gas within the block and the temporal nature of ebullition.

### ELECTROMAGNETIC MEASUREMENTS

In this work we record the travel time of an electromagnetic wave through peat blocks using commercially available ground penetrating radar (GPR) instrumentation. In our laboratory method the EM wave is transmitted at the sides/base of the peat block and the reflection from the opposite side/surface of the block (along with internal reflections due to the peat structure) is recorded.

The velocity of this EM wave ( $v$ ) in a soil is primarily controlled by the relative dielectric permittivity ( $\epsilon_r$ ) of the soil, a geophysical property strongly dependent on water content (and thus gas content). For a low-loss (non-conducting and refractive) non-magnetic medium  $v$  can be mathematically defined as:

$$v = \frac{c_0}{\sqrt{\epsilon_{r(b)}}} \quad (1)$$

where  $c_0$  is the EM wave velocity in a vacuum ( $3 \times 10^8 \text{ m s}^{-1}$ ), and  $\epsilon_{r(b)}$  is the bulk relative dielectric permittivity of the soil.

In order to estimate gas content from EM wave velocities we applied the Complex Refractive Index Model (CRIM) (e.g. [Huisman *et al.*, 2003]), which is a volumetric mixing model for the soil [West *et al.*, 2003]:

$$\epsilon_{r(b)}^\alpha = \theta \epsilon_{r(w)}^\alpha + (1-n) \epsilon_{r(s)}^\alpha + (n-\theta) \epsilon_{r(a)}^\alpha \quad (2)$$

where  $\epsilon_{r(a)}$ ,  $\epsilon_{r(w)}$ , and  $\epsilon_{r(s)}$  are the relative dielectric permittivity of gas (1), water (81) and the soil particles respectively,  $n$  is the porosity;  $\theta$  is the volumetric soil water content and  $\alpha$  is a factor accounting for the orientation of the electrical field and the geometrical arrangement of minerals (equal to 0.35 as previously reported for peat soils, Kellner and Lundin, 2001)

### EXPERIMENTAL DESIGN

A poorly decomposed *Sphagnum* peat block (0.22m x 0.32m x 0.31m) was extracted from the surface of Caribou Bog, a large, multi-unit freshwater peatland in Maine. The block was sealed, transported to the laboratory within 36 hours of extraction, and stored in an environmental chamber at 5°C until the experiment began.

Two-way electromagnetic travel-time ( $t$ ) measurements were collected daily for the first 10 days of increasing temperature, and every 2-3 days after reaching the isothermal until the end of the experiment. A Malaramac GPR system equipped with a 1.2 GHz shielded antenna was used to record  $t$  for two sets of profiles (Figure 1): a) horizontal profiles which measured the two-way travel time  $t$  horizontally across the block at three depths (lines a, b, and c); and b) vertical profiles, which measured the two-way travel time  $t$  vertically through the block at three locations (lines 1, 2, and 3).

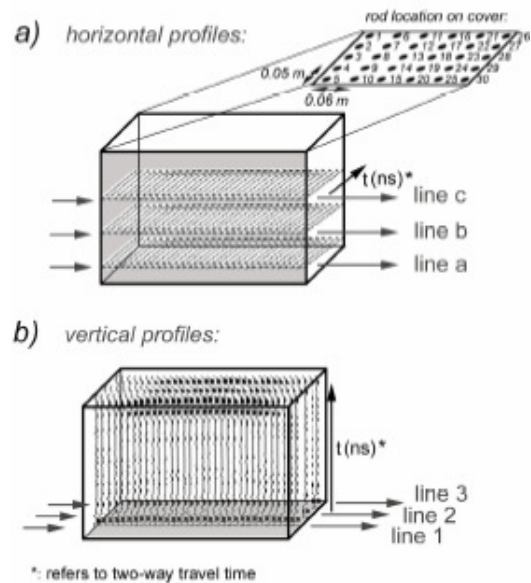


**Figure 1.** Schematic of peat sample block showing acquired GPR data along: a) horizontal profiles; and b) vertical profiles. Direction of EM wave travel time ( $t$ ) is indicated in each case and refers to two-way travel time. Schematic of rod location is also shown..

Peat surface deformation was monitored throughout the experiment using elevation rods fixed to the cover of the sample holder (inset in Figure 1a). Changes in rod

length relative to bottom of the cover were recorded for a total of 30 rods equally spaced across the surface of the sample. Biogenic gas emissions from the peat block were estimated throughout the experiment using a portable combustible gas detector (VRae) factory-calibrated for methane with a resolution of 0.1% LEL (low explosive limit, equivalent to 500 ppm of CH<sub>4</sub>). CH<sub>4</sub> fluxes were estimated by fitting a linear regression of concentration versus time and applying Henry's ideal gas law. Porosity was measured by oven drying three peat samples extracted from the center of the block at approximately similar depths.

A discrete Fourier transform was applied to all acquired data to investigate periodicities in total gas volume, surface deformation and CH<sub>4</sub> flux changes, as to explore the relative strengths of any periodic components (performed using Mathematica 4, Wolfram Research, Inc, by normalizing amplitude values by the maximum).

## RESULTS

The EM travel-time measurements reveal large shifts in biogenic gas content for all the conducted profiles. Figure 2a shows the change in gas content as a function of time (days of experiment) for GPR horizontal profiles (lines a, b, and c, in Figure 1a) obtained from application of the CRIM, using an average porosity of 94.8%, and  $\epsilon_{r(s)} = 2$ . All profiles exhibit similar behavior, with initial gas contents (at day 0) ranging between 3-6% and maximum gas contents reaching 11-12% total volume. Final gas contents correspond well with air contents as estimated from porosity analysis (ranging between 9-11% total volume). The general pattern of gas content change is also consistent between profiles, with average increases of 0.47 %, 0.50%, and 0.51% gas per day for line a, line b and line c respectively. Figure 2b shows the change in gas content as a function of time for the bottom profiles (lines 1, 2, and 3, in Figure 1b). Gas build-up and evolution is generally consistent with that obtained for the horizontal profiles (Figure 2a). Initial total gas content values (at day 0) are slightly lower, ranging between 1.5-3.5%, with maximum gas contents reaching 10% total volume. Periods of increased gas content are again well correlated between profiles, with average increases of 0.39 %, 0.42%, and 0.45% gas per day for line 1, line 2 and line 3 respectively.

Biogenic gas accumulation within the sample is evident in both the surface elevation and CH<sub>4</sub> flux data. Figure 3 shows the relative change in surface elevation (from day 0) as a function of time at three locations coincident with the location of EM bottom profiles (line 1, line 2, and line 3 in Figure 1b). All surface elevations as a function of time show a trend strikingly similar to the EM data (Figure 2 and Figure 3). From

Day 1 to Day 22 of the experiment relative increases in surface elevation average 0.73, 0.67, and 0.66 cm per day for line 1, line 2, and line 3 respectively; From Day 22 to the end of the experiment relative increases in surface elevation average 0.036, 0.022, and 0.021 cm per day for line 1, line 2, and line 3 respectively. Figure 5 shows the evolution of CH<sub>4</sub> fluxes as a function of time. The fluxes obtained are comparable to other reported values using the static chamber technique (e.g. [Strack *et al.*, 2005] reported flux values exceeding 1000 mg CH<sub>4</sub>/m<sup>2</sup>/d in a floating mat site in Canada). Although somewhat more irregular, the general trend in CH<sub>4</sub> flux corresponds with the trends shown by the EM and surface deformation measurements.

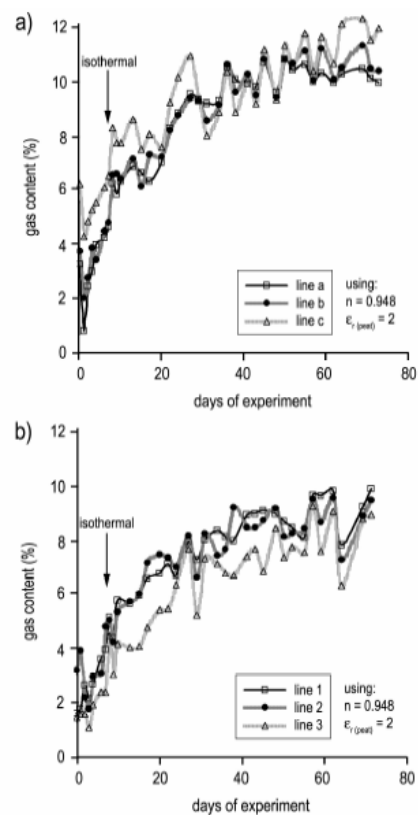


**Figure 2.** Variation of total gas content (%) volume as a function of time for a) horizontal profiles (lines a, b, and c); and vertical profiles (lines 1, 2, and 3). Porosity ( $n$ ) of 0.948 and peat relative dielectric permittivity ( $\epsilon_{r(peat)}$ ) of 2 were considered. The arrow indicates the day at which 21 °C was reached (isothermal).

Figure 5 shows the result of applying a discrete Fourier transform to the time series of horizontal EM travel time measurements at the three depths monitored (Figure 5a) and also compares vertical profile Line 2 with the surface deformation at the same location (Figure 5b). The relative amplitudes of the frequency spectrum are shown normalized to the maximum amplitude and are plotted as a function of period in

days. This frequency-domain representation of the data further illustrates the similar temporal behavior of the EM profiles and surface deformation data. The primary peak in the frequency spectrum is obviously associated with the lowest frequency sampled (72 days) and is the frequency-domain representation of the gas build up clearly observed in the time profiles (Figures 2 and 3). However, Figure 5 also reveals a distinct higher frequency signal in the temporal profiles with a period of 14 days. This signal defines the dominant periodicity in the oscillations of gas content observed in EM profiles (e.g. after the isothermal in Figure 2). Interestingly, this periodicity is strongest in the horizontal profile closest to the surface (line c) and weakest in the deepest horizontal profile (line a). Figure 7b shows that such periodicity, although muted, exists in the surface deformation pattern although with a slightly lower period of 12 days.

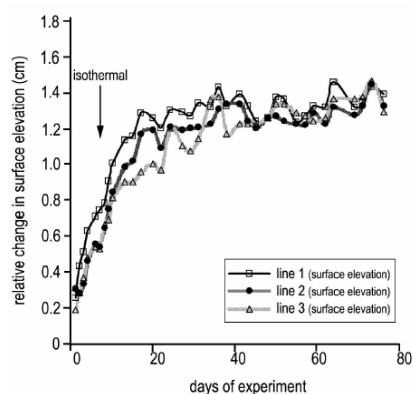


**Figure 3.** Change in surface elevation (relative to day 0) as a function of time for vertical profiles (lines 1, 2, and 3). The arrow indicates the day at which 21 °C was reached (isothermal).

## DISCUSSION

### Biogenic gas build-up and evolution

Our results for peat biogenic gas build-up and evolution are consistent with other laboratory studies (e.g. [Baird *et al.*, 2004; Strack *et al.*, 2005]). Average gas increases per day in all EM profiles show two different trends, ranging between 0.7-0.6% total volume before day 22, and 0.4-0.3% after reaching day 22 of the experiment. Low gas contents at the beginning of the experiment (between 1-6%) were expected due to the low initial temperature of the peat sample (<5 °C), that induces high gas solubilities. Maximum gas contents reached 10-12 % total volume (Figures 2) with total changes (relative to the start of the experiment) up to almost 8% as estimated from the GPR data.

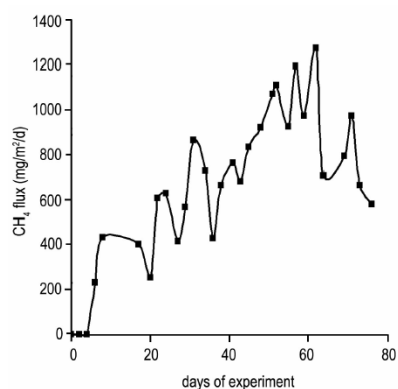


**Figure 4.** Variation of CH<sub>4</sub> flux (mg/m<sup>2</sup>/d) as a function of time in the peat block sample.

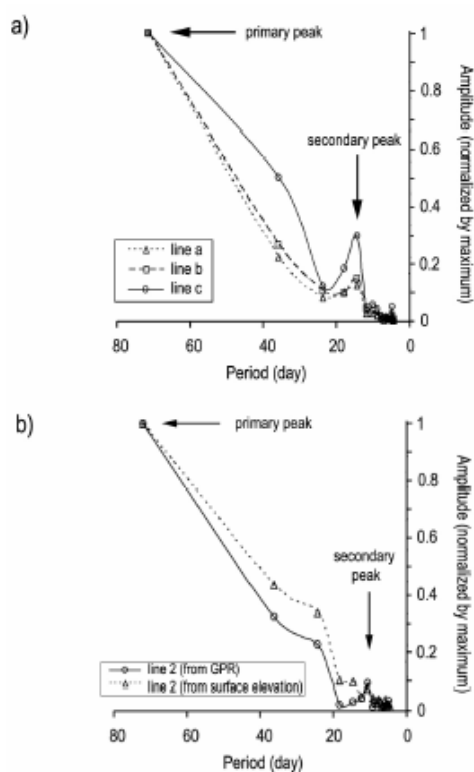


**Figure 5.** Amplitude (normalized by maximum) as a function of period (day) for: a) side or horizontal profiles (lines a, b, and c); and b) line 2 as measured from both GPR and surface deformation measurements. Arrows indicate location of primary and secondary peaks.

The most striking result in this study is the consistency between the trend in gas increases for all EM, surface deformation, and gas flux measurements. EM and surface deformation both exhibit a fairly continuous and smooth increase in gas content from day 0 up to approximately day 22. After day 22, the trend shows significant drops in gas content (and subsequent build ups) that seems consistent with the concept of ebullition. Although CH<sub>4</sub> fluxes were already detected

early after the first week of the experiment (Figure 4), the highest values were recorded after day 22 (with a maximum of  $> 1200 \text{ mg/m}^2/\text{d}$  on day 60). As previously proposed by [Baird *et al.*, 2004] peat soils may require a common storage threshold (between 10-14% total volume in their samples and after 3-10 weeks of incubation) before the main period of ebullition could occur. Although our results suggest a lower storage threshold (between 7-9% total volume), the timing for the initiation of major ebullition seems consistent (from 22 days, or around 3 weeks, until the end of the experiment).

### Biogenic gas spatial distribution

Differences on evolution of gas content at the horizontal GPR profiles (lines a, b, and c in Figure 1) may be indicative of changes in biogenic gas spatial distribution. From Figure 2a, two clear observations can be drawn: 1) gas content is overall significantly higher in line c (closer to the surface); and 2) temporal variability in gas build-up and release (e.g. ebullition) is also most pronounced in line c. These observations may suggest that most of the ebullition flux to the atmosphere is occurring from the near surface peat (with additional ebullition from depth), or more likely, the deeper layers are supplying the near surface peat region with new gas.

Increased gas content and variability closer to the surface can also be related to structural changes with depth. Peat is a porous medium with two major hydrological zones separated by the water table, the upper layer or acrotelm, and the lower layer or catotelm (Ingram, 1978). Total porosity in the acrotelm tends to decrease significantly with depth as bulk density increases due to matrix compaction (e.g. Hoag and Price, 1997). Effective porosity also tends to decrease with depth (especially in the catotelm) as higher compression and decomposition of the peat matrix tends to replace the remaining volumes with closed pores and plant material (Siegel *et al.*, 1995). Although all horizontal EM profiles were taken below the water table (and therefore can be considered from the catotelm layer), lower total and effective porosities with depth may be able to explain the higher gas content and variability over time in line c (closer to the surface). As shown in Figure 2a, higher gas contents and fluctuations in line b (middle of the sample), as compared to line a (bottom of the sample), are also congruent with this explanation.

### Periodicity of ebullition

The Fourier transform estimated from GPR and surface deformation data (Figure 7) reveals two critical observations: 1) that ebullition in our measurements exhibits some periodicity and does not seem to be

random in time (with periods between 14-12 days); and 2) that this periodicity is most pronounced in the horizontal profile closest to the surface. As shown in Figure 7a line c (closest to surface) exhibits the maximum 14 day peak, followed by line b and then line a (deepest line). This last observation is consistent with gas content change being most pronounced at the surface where the exchange with the atmosphere occurs, and seems to further suggest that the ebullition exchange with the atmosphere is primarily coming from the near surface soil.

We suggest our data may be indicative of a form of ebullition directly related to near-surface soil that seems to exhibit certain periodicity. This process is possibly associated with bog breathing (or Mooratmung) as described by Glaser, 2006, where small oscillations in topographic elevation in a raised bog in Minnesota were associated with high-frequency ebullition events. We proposed the near surface region of ebullition in our peat block may be continuously replenished by biogenic gasses being developed slightly deeper in the peat soil. Deeper layers may then be regulated by confining layers and are possibly associated with a more random ebullition.

Our work has clearly shown that EM travel time measurements offer unique, non-invasive, means to explore gas dynamics in peat soils. It is important to note that the technique could readily be deployed in the field, for example by measuring changes in the two-way travel time from the surface to prominent reflectors e.g. the peat-inorganic soil horizon. With this approach ebullition events driven by changes in atmospheric and/or hydrostatic pressure could be investigated.

## CONCLUSIONS

This study shows the potential of EM travel-time measurements as a non-invasive technique to image the evolution, spatial location and emission patterns of biogenic gasses in a peat block. GPR and surface deformation measurements revealed consistent shifts in biogenic gas content. We demonstrated that EM travel time measurements are a totally non-invasive way of investigating gas dynamics without risking alteration of gas dynamics (e.g. by insertion of probes). Our measurements on peat blocks show many consistencies with previous studies of gas dynamics in peat soils including critical gas volumes (or thresholds) to initiate ebullition. Under our experimental conditions, ebullition appears to preferentially occur from the near-surface peat, and is possibly associated to bog breathing (or Mooratmung) as described by others. This ebullition shows certain periodicity, suggesting it could be predictable and might allow this ebullition flux to be incorporated into global climate models.

## ACKNOWLEDGEMENTS

This material is based upon work supported by the National Foundation under grant No. 0510370. Rutgers University graduate students Mike O'Brien, Jay Nolan, and Maitry Roy-Moulik provided valuable field and lab support. We are especially thankful to Andrew Reeve (University of Maine) for field support and for his continuous collaboration on peatland research, and Andrew Baird for valuable discussions regarding laboratory-based experiments on peat blocks

## REFERENCES

- Baird, A. J., C. W. Beckwith, S. Waldron, and J. M. Waddington (2004), Ebullition of methane-containing gas bubbles from near-surface *Sphagnum* peat, *Geophysical Research Letters*, *31*, L21505.
- Baird, A. J., and S. Waldron (2003), Shallow horizontal groundwater flow in peatlands is reduced by bacteriogenic gas production, *Geophysical Research Letters*, *30*, 2043.
- Beckwith, C. W., and A. J. Baird (2001), Effect of biogenic gas bubbles on water flow through poorly decomposed blanket peat, *Water Resources Research*, *37*, 551-558.
- Comas, X., L. Slater, and A. Reeve (2005b), Spatial variability in biogenic gas accumulations in peat soils is revealed by ground penetrating radar (GPR), *Geophysical Research Letters*, *32*, L08401.
- Fechner-Levy, E. J., and H. F. Hemond (1996), Trapped methane volume and potential effects on methane ebullition in a northern peatland, *Limnol. Oceanogr.*, *41*, 1375-1383.
- Glaser, P. H., J. P. Chanton, P. Morin, D. O. Rosenberry, D. I. Siegel, O. Ruud, L. I. Chasar, and A. S. Reeve (2004), Surface deformations as indicators of deep ebullition fluxes in a large northern peatland, *Global Biogeochemical Cycles*, *18*, GB1003.
- Glaser, P. H. (2006), An Overview of gas ebullition and bog breathnig (Mooratmung) in Northern Peatlands, EOS Trans. AGU, 87 (36), Jt. Assem. Suppl., Abstract NS24A-02.
- Huisman, J. A., S. S. Hubbard, J. D. Redman, and A. P. Annan (2003), Measuring soil water content with ground penetrating radar: a review, *Vadose Zone Journal*, *2*, 476-491.
- Hoag, R. S. and J. S. Price (1997), The effects of matrix diffusion on solute transport in undisturbed peat in laboratory columns, *J. Contaminant Hydrology*, *28*, 193-205
- Ingram, H. A. P (1978). Soil layers in mires: function and terminology. *J. Soil Sci.*, *29*: 213-218.
- Kellner, E., and L. C. Lundin (2001), Calibration of time domain reflectometry for water content in peat soils, *Nordic Hydrology*, *32*, 315-332.
- Kellner, E., J. M. Waddington, and J. S. Price (2005), Dynamics of biogenic gas bubbles in peat: Potential effects on water storage and peat deformation, *Water Resources Research*, *41*, W08417.
- Khalil, M. A. K. (2000), *Atmospheric methane, Its role in the global environment*, Springer-Verlag, New York.
- Romanowicz, E. A., D. I. Siegel, J. P. Chanton, and P. H. Glaser (1995), Temporal variations in dissolved methane deep in the Lake Agassiz Peatlands, Minnesota, *Global Biogeochemical Cycles*, *9*, 197-212.
- Rosenberry, D. O., P. H. Glaser, D. I. Siegel, and E. P. Weeks (2003), Use of hydraulic head to estimate volumetric gas content and ebullition flux in northern peatlands, *Water Resources Research*, *39*, 1066.
- Siegel, D. I., A. S. Reeve, P. H. Glaser, and E. A. Romanowicz (1995), Climate-driven flushing of pore water in peatlands. *Nature*, *374*: 531-533.
- Strack, M., E. Kellner, and J. M. Waddington (2005), Dynamics of biogenic gas bubbles in peat and their effects on peatland biogeochemistry, *Global Biogeochemical Cycles*, *19*, GB1003.
- Tokida, T., T. Miyazaki, and M. Mizoguchi (2005a), Ebullition of methane from peat with falling atmospheric pressure, *Geophysical Research Letters*, *32*, L13823.
- Tokida, T., T. Miyazaki, M. Mizoguchi, and K. Seki (2005b), In situ accumulation of methane bubbles in a natural wetland soil, *European Journal of Soil Science*, *56*, 389-396.
- West, J. L., K. Handley, Y. Huang, and M. Pokar (2003), Radar frequency dielectric dispersion in sandstone: Implications for determination of moisture and clay content, *Water Resources Research*, *39*, 1026.
- Whalen, S. C., and W. S. Reeburgh (1992), Interannual variations in tundra methane emissions: A 4-year time series at fixed sites, *Global Biogeochemical Cycles*, *6*, 139-159.

## **Electromagnetic imaging of deep basement grabens for sustainable regional groundwater development in the eastern margin of Parnaíba basin, Brazil**

Sergio Fontes , Observatorio Nacional-MCT, Rio de Janeiro, Brazil

Max Meju, Department of Environmental Science, Lancaster University, Lancaster LA1 4YQ, UK

---

### **SUMMARY**

A combined TEM-AMT survey was carried out along three east-west transects at the eastern margin of Parnaíba basin for hydrogeological purposes. The MT data were processed using conventional tensorial analysis technique and corrected for static shift using dual-mode TEM data. Two-dimensional regularised inversion of the TE and TM MT data revealed distinct geoelectric patterns for the three profiles. The contact between the sedimentary and crystalline basement rocks was clearly imaged on the three profiles in the area of study. Graben-like structures were observed on the Monsenhor Hipólito, Jaicós and Itainópolis transects. A major fault, interpreted as the Picos fault, was imaged on the Monsenhor Hipólito transect and may have implications for groundwater flow in the area. The graben structures were suggested as the best places for deep drilling for groundwater in this region. Follow-up >800m deep drilling guided by our models was highly successful and establishes MT conductivity imaging as a vital tool for groundwater development and resource sustainability studies in this semi-arid region.

**Keywords:** Magnetotelluric imaging, basement grabens, deep aquifers, sustainable groundwater development

---

### **INTRODUCTION**

Previous regional TEM-MT studies in southern parts of Piauí state, within the Parnaíba basin in Brazil, detected zones of anomalously thickened basement cover units interpreted as possible grabens east of Picos (see Meju et al., 1999, Fig. 18) and north of São Raimundo Nonato (see Fontes et al., 1997). One of these anomalous graben structures was recently drilled down to 970m and found to contain a prolific aquifer; it now serves as the main water supply for São Raimundo Nonato located 35 km away from the borehole site. Based on these studies, the Piauí state government embarked on a programme to map out potential future sources of groundwater for the urban populations near the eastern margin of Parnaíba basin. The area is semi-arid and the rainfall is low (<400mm per year). It was decided, particularly in the case of Monsenhor Hipólito (MH) and environs reported here, that deep electromagnetic tracking of the previously suggested graben near Picos should be undertaken to

confirm its existence and along-strike continuity to aid groundwater resource evaluation.

The geology of the study area is made up of sequences of sedimentary rocks resting on crystalline basement. The sedimentary rocks outcropping in the study area are shown in Figure 1. The Serra Grande group rests on the Precambrian crystalline basement. This group consists successively of the Jaicos, Ipu and Tiangua formations. The Jaicos formation is the dominant member and the target aquifer in the area. The Serra Grande group is overlain by the Pimenteiras formation, which is the main aquitard. It is overlain in turn by the Cabeças formation outside the area of study.

### **FIELDWORK AND RESULTS**

#### **Data acquisition, processing and interpretation**

Joint TEM and AMT soundings were carried out in the area of investigation. The survey consisted of three east-west lines as shown in Figure 1. Profile 1 - Monsenhor Hipólito profile - is 64 km long and there

are ten stations with an average spacing of 6.4 km. Profile 2 - Jaicós profile - is 23 km long, consisting of nine stations and with an average spacing of 2.5 km. Profile 3 - Itainópolis profile - is 40 km long with ten stations spaced of 4 km apart on average. Central-loop and single-loop TEM data were acquired at all sites using either 50 or 100 m-sided transmitter loops. The Sirotem MK3b system was used for the TEM soundings. The MT measurements employed the EMI MT-1 field equipment with 100m telluric dipoles.

The MT data were processed using a robust estimation technique (Egbert and Booker, 1986) and the relevant interpretative parameters were computed for the sounding frequency range 336 to 0.14 Hz. Distortion decomposition and structural dimensionality were determined for the various sites using the Groom-Bailey technique (1989). The computed azimuths at some selected frequencies suggest a dominant strike for each profile. It is nearly north-south for the Monsenhor Hipólito profile; this is orthogonal to the direction of the survey line and is consistent with the main geological trend. Subsequently, the data were rotated  $30^{\circ}$  from the measurement direction (the declination is  $23^{\circ}$  west of geographic north) yielding the TE and TM modes along approximately north-south and east-west directions, respectively. The other 2 profiles were rotated  $70^{\circ}$ , a direction which is also in agreement with the trend of the main regional faults. The TM and TE mode apparent resistivity curves were respectively corrected for static shift using the single-loop and central-loop TEM data (cf. Meju et al., 1999). A conjugate gradient 2-D non-linear inversion program (Rodi and Mackie, 2001) was applied to the corrected MT TM and TE data. The main results for each profile are described below.

#### **Monsenhor Hipólito Profile**

The 2-D model (Figure 2) suggests the presence of strong lateral changes in resistivity in the top 4.5 km of this profile. The basement units are generally highly resistive and a value of  $\rho \geq 200$  ohm-m appears to be appropriate for them. These units outcrop on the surface at stations 9 and 10. The relatively conductive zone near the surface at station 9 may thus indicate the presence of highly weathered basement rocks. The basement appears to be of irregular topography and is overlain by thickened sedimentary cover at stations 1 and 2 and between stations 3 and 5. The contact between the basement and its sedimentary cover may be traced westward along the profile starting at a position between stations 8 and 9 (in agreement with the basement-sediment contact on the geological map shown in Fig. 1). The Serra Grande group aquifer (dominantly the Jaicos formation in this study area) outcrops at stations 3 to 8 and appears to be well imaged by the resistivity inversion model. This segment of the model is the recharge area. The

Pimenteiras shale formation, an aquitard, forms the confining layer west of this recharge zone. There appears to be a resistive sill-like body underneath profile positions 0-5 km in agreement with the MT model for an earlier parallel profile running from Sao Juliao through Picos to the west (Meju et al., 1999).

The 2-D model also shows other interesting geological features. A major fault is suggested near station 2 and extends vertically into the basement. The fault appears as a highly conductive zone and may represent the edge of major graben structure or have hydraulic link with a caldera found just south of Picos (Fig. 1). The smaller graben suggested between profile position 15 and 25 km agrees with that seen previously on Jaicos-Picos transect (Ulugergeli, 1998). This particular graben appears to contain thick sedimentary materials, possibly of the Serra Grande Group. We recommended that the area between profile position 15 and 25 km has the optimum potential for deep drilling for groundwater since the deeper graben-like zone at position 0-5 km may contain saline groundwater.

#### **Jaicós Profile**

The 2D model in Figure 3 suggests a shallower conductive sedimentary cover along the Jaicós profile than the Monsenhor Hipólito profile. There appears to be a minor graben or depression-storage zone between profile positions 6 and 14 km. We identified this zone as the optimum site for deep drilling for groundwater.

#### **Itainópolis Profile**

The 2-D model in Figure 4 shows appreciable lateral resistivity changes and a graben structure near the center of the profile (position 13-17 km) which we identified as the most appropriate site for deep drilling for groundwater.

### **CONCLUSION**

Based on the present results, it would appear that the MT conductivity imaging is an effective tool for structural and stratigraphic mapping in this region. It has been shown that the contact between the basement and sedimentary cover can be discerned from the MT images. A possible graben like-structure is also clearly delineated in the images. The imaged grabens on two of these transects have now been successfully developed for water supply. The Jaicos profile is yet to be drilled. We suggest that the recharge areas for the main Serra Grande aquifer can be mapped and used to control groundwater development and land use pattern leading to sustainable development in the area of study.

### **ACKNOWLEDGEMENTS**

This work was supported by Secretaria de Meio Ambiente e Recursos Hídricos do Piauí, PROAGUA project.

**REFERENCES**

Egbert, G.D. and Booker, J.R., 1986, Robust estimation of geomagnetic transfer functions, *Geophys. J.R.astr. Soc.*, 87, 173-194.

Fontes, S.L., Meju, M.A., Lima, J.P.R., Carvalho, R.M., La-Terra, E.F., Germano, C.R., and Metelo, M., 1997, Geophysical investigation of major structural controls on groundwater distribution, North of Sao Raimundo Nonato, Piaui. 5<sup>th</sup> International Congress of the Brazilian Geophys. Soc., Sao Paulo, Expanded Abstract, Vol.2, 766-769.

Groom, R.W., and Bailey, R.C., 1989, Decomposition of magnetotelluric impedance tensors in the presence

of local three-dimensional galvanic distortion, *J.Geophys. res.*, 94, 1913-1925.

Meju, M.A., Fontes, S.L., Oliveira, M.F.B., Lima, J.P.R., Ulugergerli, E.U., Carrasquilla, A.A., 1999, Regional aquifer mapping using combined VES-TEM/EMAP methods in the semiarid eastern margin of Parnaiba Basin, Brazil, *Geophysics*, 64, 1-20.

Rodi W., and Mackie R.L., 2001. Nonlinear conjugate gradient algorithm for 2-D magnetotelluric inversion. *Geophysics*, 66, 1, 174-187.

Ulugergerli, E.U., 1998, Development and application of 2-D magnetotelluric inversion in complex domain, PhD thesis, University of Leicester, UK.

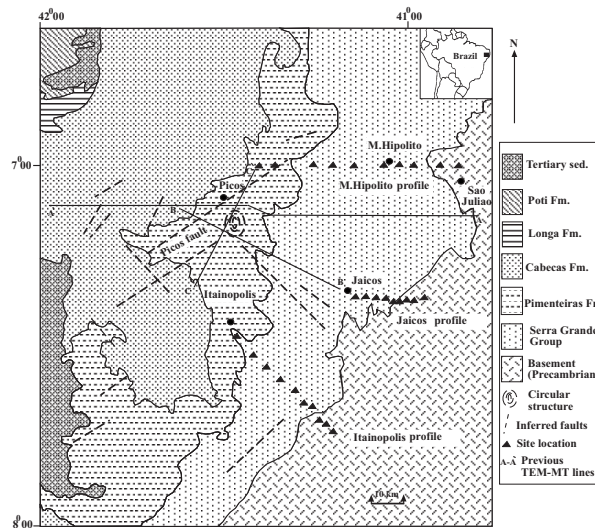


Figure 1. Geological map of the area of study showing the TEM-MT site locations.

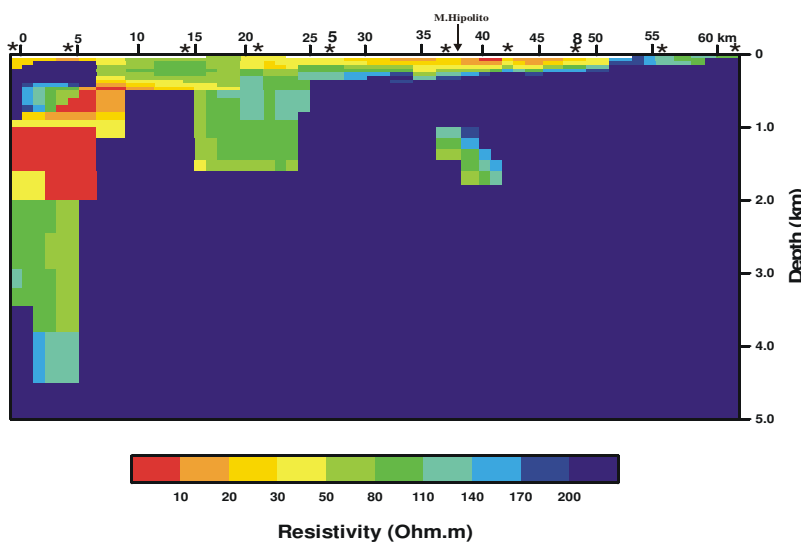


Figure 2. Resistivity structure for the Monsenhor Hipólito profile derived from 2-D MT inversion.

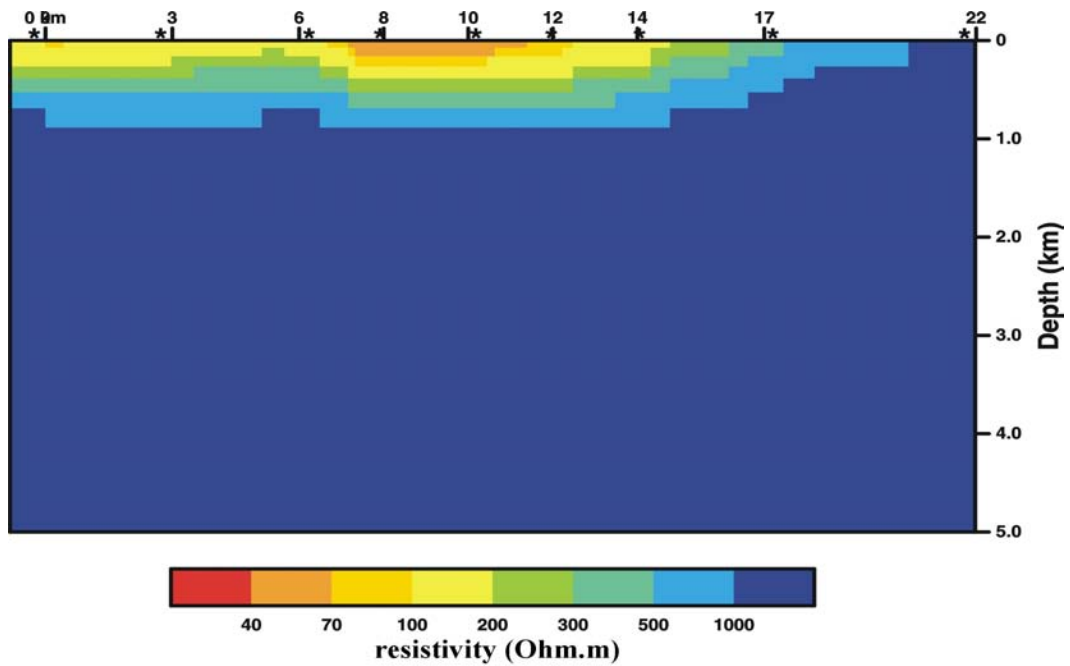


Figure 3. Resistivity structure for the Jaicós profile derived from 2-D MT inversion.

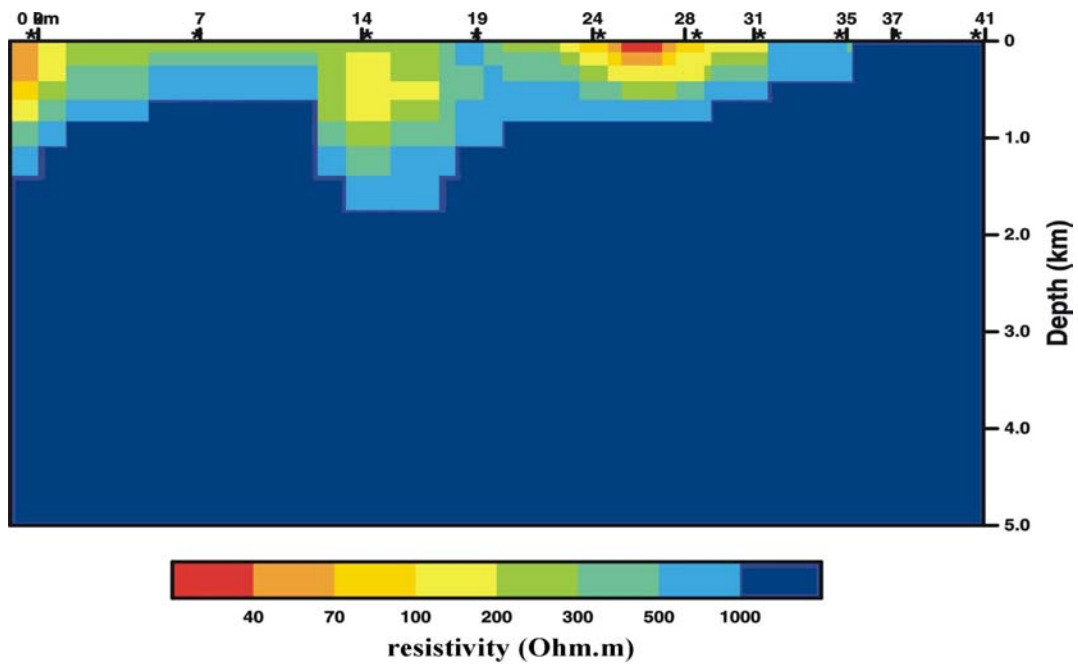


Figure 4. Resistivity structure for the Itainópolis profile derived from 2-D MT inversion.

## Inversion of Continuous Wave Metal Detector Data using Spheroids

Joern Lange, University of Cologne, Institute for Geophysics and Meteorology, Cologne, Germany  
 Tilman Hanstein, Harbourdom GmbH, Cologne, Germany  
 Stefan L. Helwig, University of Cologne, Institute for Geophysics and Meteorology, Cologne, Germany

### SUMMARY

We show the interpretation of Continuous Wave metal detector signals with a Marquardt-Levenberg inversion. The forward solver calculates the response of a conductive and magnetic spheroid approximated by spheres with different excited dipole moments. For the exact simulation of the used CW-detector the exact shape of its coils is considered as well as the gains for both used frequencies. To compensate the influence of static magnetic soil only the weighted differences of the measured imaginary parts and both of the real parts are used. To get a good initial guess for the model the ratio of the two real parts is used. Its behavior gives information about the shape and the orientation of the spheroid. With this procedure most of the investigated mine surrogates can be interpreted and their depth can be determined.

**Keywords:** Metal Detectors, Inversion, Spheroids

### INTRODUCTION

Metal detectors are the most used devices when searching for land mines. The information the detector delivers is mostly limited to the signal strength, which can be related to the distance, size, conductivity or permeability of the object. To get more information out of the signal and to reduce the false alarm rate the German Federal Ministry of Education and Research funds the project network "HuMin/MD Metal detectors for Humanitarian Demining: Development potentials for data analysis and measurement techniques", where eleven institutes are involved working on 3D-imaging, signal analysis, research on the soil influence and the measurement technique.

The investigated metal detectors are similar to the time- and frequency domain electromagnetic measuring devices in geophysics. In the transmitter coil an alternating or pulsed current excites a primary magnetic field, which causes induction current in the conducting vicinity, particularly in metal objects. These currents generate a secondary magnetic field which is detected with one or more receiver coils. Depending on the excitation current a distinction is drawn between pulse induction (PI) and continuous wave (CW) metal detectors.

Our approach to interpret the signal is the inversion of the measured data with a fast semi-analytical calculation for simple objects like spheres, rings and spheroids. For the latter Smith and Morrison (2006) introduced an approximation based on spheres, which can be calculated very fast compared to the exact solution. It is accurate for moderate aspect ratios of the semi axis (0.25-4). Exact solutions can be calculated for small spheres compared to the diameter of the transmitter coil. We use them to test and calibrate our inversion.

In the following the inversion of data measured with a CW metal detector in the laboratory is shown. The used device is a Foerster Minex 2FD 4500, which works with two frequencies, namely 2.4 kHz and 19.2 kHz.

### SIMULATION

The response of a sphere with radius  $a$  in a homogeneous magnetic field  $\mathbf{H}_P$  in cylinder coordinates  $R, \theta$  and  $z$  with origin at the center of the sphere can be expressed by (Wait (1951)):

$$H_R = \frac{Da^3}{R^3} H_z^p \cos(\theta) \quad (1)$$

$$H_\theta = \frac{Da^3}{2R^3} H_z^p \sin(\theta) \quad (2)$$

with complex reflexion factor  $D$ :

$$D = \frac{(2\mu_s/\mu_g + 1)x - [(\mu_s/\mu_g + 2) + x^2] \tanh(x)}{(\mu_s/\mu_g - 1)x + [(1 - \mu_s/\mu_g) + x^2] \tanh(x)} \quad (3)$$

where  $\mu_s$  and  $\mu_g$  are the magnetic permeability of the sphere and the surrounding medium,  $x = a\sqrt{i\sigma\mu_s\omega}$  the complex induction number,  $\sigma$  the conductivity of the sphere and  $\omega$  the frequency. The field of the homogenous ground can be added since the depth of the sphere is much less than one skin depth of the primary field.

As long as the permeability of the ground is not frequency dependent their influence will only be visible in the real part of the received magnetic field and accordingly in the imaginary part of the voltage  $i\omega\mu\mathbf{H}$  induced in the receiver coil.

To suppress the influence of the magnetic ground in the signal it is useful to measure with at least two different frequencies. For the interpretation only the frequency weighted difference of the imaginary parts of the induced voltage measured at two different frequencies and the two real parts are used, as these are not influenced by static magnetic permeability. In contrast the secondary field of the sphere is frequency dependent, so that their response will still be seen.

The strength of the dipole moment of the sphere  $\mathbf{M} = 2\pi a^3 D \mathbf{H}^p$  is not depending on the direction of the primary field. For a spheroid with semi axis  $a$  and  $b$  ( $a$  parallel to the axis of rotation) this is different. In the used approximation by Smith and Morrison (2006) the response of a magnetic and conductive spheroid is described by two polarizabilities, one parallel and the other one perpendicular to the axis of rotation. For a magnetic prolate spheroid ( $a > b$ ) the parallel polarizability is bigger and for the magnetic oblate spheroid ( $a < b$ ) the perpendicular one. Both are expressed as scaled sphere polarizabilities which are the ratio of the dipole moment and the external magnetic field.

The primary field is calculated by parameterising of the exact coil shape (figure 3) and using Biot Savards law.

### FINDING A STARTING MODEL

It is known that for a Marquardt-Levenberg inversion scheme the initial guess is important to find the global minimum. For this reason we use a two step procedure to get the starting model. In the first step the

shape and orientation of the object, as long it can be fitted with a magnetic and conductive spheroid, is determined. Therefore we use the ratios of the different channels as they are independent of the amplitude of primary field. The investigated metal detector uses two frequencies 2.4 kHz and 19.2 kHz. The three channels we use in our interpretation are the real parts of the signal for both frequencies (Re1 and Re2) and the difference of the imaginary part of the signal for the two frequencies (Im1-Im2). Since the induced voltages are proportional to the frequency and we are interested in the dipole moment the real- and imaginary parts are normalized by their frequency.

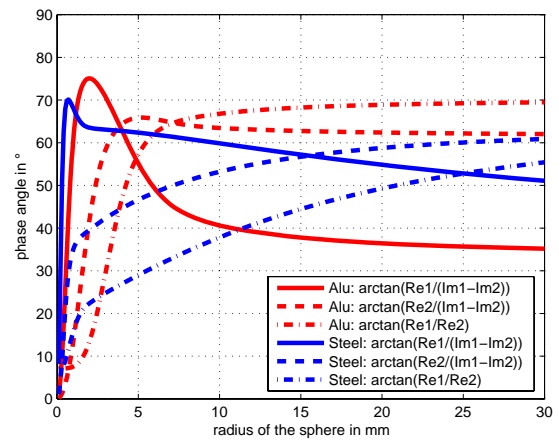


**Figure 1.** Ratios of the three channels expressed in terms of a phase angle for a aluminium and a steel sphere as a function of the sphere radius. The Channels are the real parts of the signal for 2.4 kHz and 19.2 kHz (Re1 and Re2) normalized by the frequency, and the difference of the normalized imaginary parts (Im1-Im2).

Figure 1 shows the ratios of the three channels in terms of phase angles for a steel and an aluminium sphere as a function of the sphere radius. Each of them can be used for signal analysis. As can be seen in the figure and can be calculated with equation 3  $\arctan(Re1/Re2)$  is the only phase angle which is monotonically increasing with increasing radius and so with increasing dipole moment. For an object like a spheroid, with two different dipole moments for different excitation directions this monotonically behavior can be used to determine which of the different dipole moments is the biggest. Depending on the position of the spheroid in respect to the detector the one is more excited then the other and because of this, different phase angles of Re1/Re2 are measured.

In figure 2 the different excitations are illustrated. For an oblate orientated with the rotation axis parallel to the z-direction (lower, right) minimum phase angle is measured directly above the spheroid. If the detector is moved in x- or y-direction the phase angle will increase. For each orientation and shape of the spheroid there is a typical behavior of this parameter which allows an identification. For non magnetic spheroids the relation of the dipole moments is vice versa. Therefore this procedure works only for magnetic spheroids.

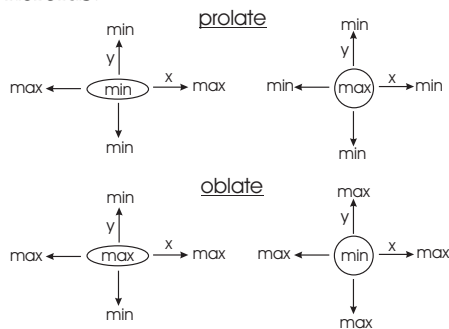


**Figure 2.** Excited dipole moments for oblate and prolate spheroids, when the detector is moved out of the central position above the spheroid.

In the second step of the initial model search, a spheroid with fixed ratio of the semi axis and fixed orientation is varied in depth, size, conductivity and magnetic permeability and the one which fits the data best is chosen as a starting model. At the moment the total number of tested models is 18, which takes less time then needed for one iteration.

**INVERSION OF LABORATORY AND FIELD DATA**

The measurements within the project are done by the Institute for Electrical Engineering of the University of Rostock in the laboratory and by the Fraunhofer Institute for Nondestructive Testing in Saarbruecken in the test field in Ispra/Italy.

A scheme of the used FD-Detector is shown in figure 3. It consists of a transmitter coil and two differential wound receiver coils which are symmetric arranged within the transmitter. The exact size and the amplifiers were determined by an inversion of data sets measured over spheres, whose parameters were well known.

Figure 3 gives an example of the signal measured in the laboratory. The object is an aluminium sphere with 2.8 cm diameter 5 cm underneath the detector at x = 28 cm in air. As there is no magnetic ground, all four measured parts are shown.

Because directly above the sphere the induced voltage in both of the receiver coils is the same, the resulting difference is zero in every channel. Offside of the center the induced voltage either in the left or the right receiver coil is bigger and the resulting difference therefore positive or negative.

The solid lines show the resulting data from the inversion of Re1, Re2, Im1 and Im2. The received model agrees well for depth and size of the sphere (radius=13.9 mm, depth=5.08 cm) and also for conductivity and permeability. Taking a spheroid as a model the result gets worse but is still quite accurate (a=12.8 mm, b=14.7 mm, depth=5.1 cm).

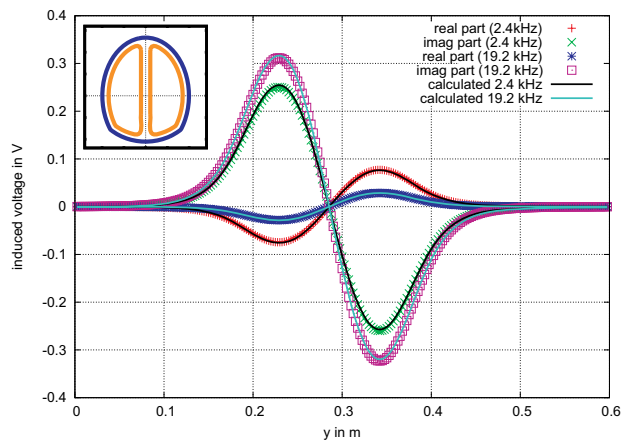


**Figure 3.** Measured and calculated voltages of the detector for a profile 5 cm above the center of a aluminium sphere with 2.8 cm diameter. Upper left: transmitter and receiver coils of the Foerster Minex 2FD 4500.

For the interpretation of field data or more complex models the inversion of Re1, Re2 and Im1-Im2 is preferable. Besides the effect of eliminating the static magnetic soil influence, tests show that more complex metal part combinations can be fitted. A reason could be that the imaginary parts for non-magnetic and magnetic spheres have a different algebraic sign, but Im1-Im2 have all the time the same, independent of the magnetic property of the sphere. At the moment we do further investigations on this with numerical simulations.

An example of the inversion of a mine surrogate is displayed in figure 4. The used data set was measured in the laboratory and consist of four profiles. Shown is the one directly above the object. The metal parts of the mine surrogate M1A are shown in the upper right picture. It consists of a spring (steel, 18 mm long, 6 mm diameter), a screw (steel, 6 mm long, 3 mm di-

ameter) and a capsule (aluminium, 8 mm long, 6 mm diameter). As can be seen the agreement of the measured and calculated data is very good. The resulting spheroid has a conductivity of  $4.1 \text{ MS/m}$ , a  $\mu_r$  of 2,  $a = 4.3 \text{ mm}$  and  $b = 3.6 \text{ mm}$ . The rotation axis of the spheroid is nearly ( $4^\circ$ ) parallel to the z-axis. Its depth agrees with the depth of the screw. For other depth of the surrogate we get the same results, so that it can be assumed that this spheroid is typical for the M1A.

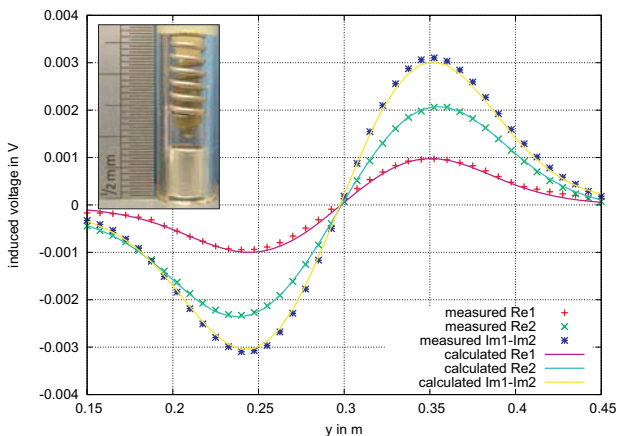


**Figure 4.** Measured and calculated voltages of the detector for a profile 2.5 cm above the center of the mine surrogate M1A. Upper left: metal parts of M1A.

If the one semi axis of the spheroid is much bigger than the other one, e.g. ( $a \gg b$ ) and  $a$  is perpendicular to the z-direction and to the symmetry axis of the detector the signal will have more than one sign reversal. Directly above the spheroid the smaller moment is excited. When the detector is moved the larger moment will be increasingly excited while the primary field decreases. For  $a \gg b$  the first process will overbalance the second one and cause an additional sign reversal.

The mine surrogate M3B which is representative for some common land mines causes such a signal (figure 5). For the measurements, which were done in Ispra/Italia on a test field, the detector was moved 7 cm above the ground (pure sand). Again only the profile directly above the M3B (in 10 cm depth) is shown, although the data set consists of 9 parallel profiles. The main parts of the surrogate are the aluminium capsule (same as in M1A) and a striker (M6x65mm coach bolt and nut). The spheroid which results from the inversion has the parameters  $a = 5.5 \text{ cm}$ ,  $b = 4.2 \text{ mm}$ ,  $7.6 \text{ MS/m}$ ,  $\mu_r = 47$ , depth = 12.05 cm and its rotation axis is parallel to the y-axis, which is the same orientation as the striker has. The aspect ratio of the spheroid is 13 and therefore the used forward approximation is no longer ac-

curate. This is the reason why the longer semi-axis exceeds the dimensions of the striker. Measurements for different spacing of the detector and the mine showed, that this aspect ratio is typical for the M3B.

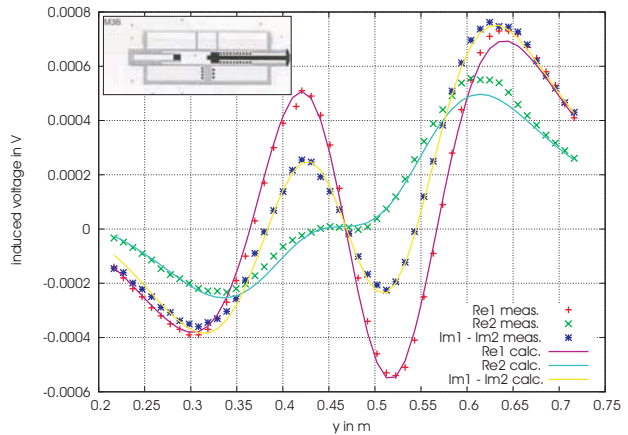


**Figure 5.** Measured (field data) and calculated voltages of the detector for a profile 17 cm above the center of the mine surrogate M3B. Upper left: sketch of the M3B (height: 5 cm, diameter: 11 cm), metal parts are drawn in black.

The inversion was also tested on data measured over other objects in the test field in Ispra/Italia. For the greater depths of the objects the data quality gets worse, so that there is a detection, but no deeper analysis is possible. For the other objects the results were quite reasonable and allowed in most of the cases an identification of the object (if the typical spheroids are known) and its depth.

## CONCLUSIONS

When the static magnetic soil effect is suppressed by building the weighted difference of the imaginary parts of the two frequencies also objects composed of different metal objects can be fitted with a spheroid. The results give a good estimate of the depth, size and material of the detected object. Without taking the difference of  $\text{Im}1$  and  $\text{Im}2$  more complicated models are needed to explain the measured signal. An inversion with such models would take much longer and is less stable.

## REFERENCES

- Smith, J. T., and Morrison, H. F., 2006, Approximating spheroid inductive responses using spheres: *Geophysics*, **71**, G21–G25.
- Wait, J. R., 1951, A conducting sphere in a time varying magnetic field: *Geophysics*, **16**, 666–372.

## S6-E8

*IAGA WG 1.2 on Electromagnetic Induction in the Earth  
Extended Abstract 18<sup>th</sup> Workshop  
El Vendrell, Spain, September 17-23, 2006*

---

### GROUND-BASE MONITORING SYSTEM OF THE LANDSLIDES ASSOCIATED WITH SEISMIC EVENTS

Maria Stanica, Dumitru Stanica, Constantin Diacopolos, and Marian Popescu  
Institute of Geodynamics of the Romanian Academy, 19-21, Jean-Louis Calderon St.,  
Bucharest, Romania

---

#### SUMMARY

The paper is centered on the establishing of a specific methodology useful for the natural hazard assessment due to both the active faults and seismic events associated, which are considered to be sources of the significant landslides in the Subcarpathian area (Romania). Thus, in the Provita de Sus zone cross-cut by active faults orientated NE-SW, the Provita Fault has been reactivated by the intermediate depth earthquakes (M=6) occurred in the Vrancea zone, on 27-th November 2004. This landslide deforms the sliced blocks considerably and produces a complex array of reverse micro-faults, strike-slip micro-faults and folds. Owing to an increasing threat of the landslides, it was necessary to choose an adequate monitoring system taking into account the specific geological conditions. In this context, an adapted electromagnetic methodology conveying to models concerning the evolution in time of the landslide phenomena was imposed, so that a disaster forecasting become possible. On this way, by using a specific ground-base monitoring system, the following activities have been accomplished: (i) optimization of the specific sensors structure in laboratory and field conditions; (ii) experiment and continuous improvement of the specific ground-base monitoring system at the peculiar conditions of the Provita de Sus (test site) for pattern recognition; (iii) getting of the specific data to produce two-dimensional tomographic images as a first step for the risk assessment; (iv) assessment of the electromagnetic parameters related to both the earthquakes characteristic to the seismic-active Vrancea zone and the landslides associated to the active fault. The final results highlight the possibility of merging electromagnetic parameters with tomographic images and with low frequency electric signals occurred prior the stress to reach a critical value. Subsequently, in the Provita de Sus locality, after implementing this complex monitoring system, it is possible to provide early-warning against the risk arising from landslide triggered by the earthquakes occurred in the Vrancea zone.

**Keywords:** landslide, active fault, electromagnetic parameters, two-dimensional images, Provita de Sus-test site.

---

#### INTRODUCTION

Landslides commonly occur with other natural disasters (earthquakes or floods) and leave the landscape prone to sedimentation, erosion and further mass wasting. The rapid development of various techniques, such as GPS (Malet et al., 2002;), GPS and digital photogrammetry (Mora et al., 2003), high-resolution satellite imagery (Haerberlin et al., 2004) and light detection and ranging (McKean and Roering, 2004), were successfully applied for continuous observation under real field conditions. Since each landslide is different, it was necessary to choose an adequate monitoring system on the basis of the preliminary analysis of a phenomenon and geological conditions (Stanica and Zugravescu, 2004; Stanica et al., 2004; Stanica et al., 2005). The goal of the paper is to present a specific ground-base monitoring system

(SGMS), to better understand its efficiency for broad application in landslide studies and hazard mitigation. Additionally, by combining different data types and analysis techniques, and also by merging electromagnetic parameters with tomographic images and with low frequency electric signals occurred prior the stress to reach a critical value, a compelling dynamical paradigm, in which is emphasized a correlation between electromagnetic parameters and the frequency and the magnitude of the occurred earthquakes, was carried out. In consequence, by analyzing the data from the Provita de Sus (test site), it was possible to assign the increase of the landslide activity to the local fault which has been reactivated by the earthquakes (EQ) occurred in the Vrancea zone. In the end, this paper illustrate the stage of the SGMS implementation and to what extent the results carried out in the Provita de Sus test site, Prahova District,

may contribute on understanding such kind of landslide.

### PROVITA DE SUS LANDSLIDE

#### Geological characteristics.

In the Provita de Sus landslide area cross-cut by active faults orientated NE-SW, the Provita Fault (PF) has been reactivated by the intermediate depth earthquakes (M=6) occurred in the Vrancea seismic-active zone, on 27-th November 2004, and has been developing in the flyschoid domain of the Subcarpathians. The Provita landslide has following characteristics:

- both the rear and front limits of the slide deposits are at about 670 m and at 410 m altitude, respectively;
- the maximum thickness of the slide deposits is of about 35 m;
- the angle of rupture surface is about 30° (rear) and 10° (front);
- the landslide area is about 1.25 km<sup>2</sup>.

#### SPECIFIC GROUND-BASE MONITORING SYSTEM (SGMS)

One of the main objectives of this paper was to implement a complex monitoring system able to provide early-warning against the risk arising from landslide triggered by the EQ occurred in the Vrancea zone, in this particular case concerning the Provita de Sus locality. In this respect, a methodology able to investigate the electromagnetic and electric parameters induced by the crustal and subcrustal geodynamic processes (landslides triggered by earthquakes) will be presented (Stanica et al., 2005). The main activities that have been accomplished consist of: (i) study regarding the optimization of the electric sensors; (ii) experiment and continuous improvement of the monitoring system at the peculiar conditions of the Provita de Sus (test site) for pattern recognition; (iii) getting of specific data to produce 2D tomographic images as a first step for the risk assessment; (iv) assessment of the electromagnetic parameters related to both the earthquakes (EQ) occurred at the intermediate depth, characteristic to the seismic-active Vrancea zone, and the landslides associated to the Provita active fault (PF). The SGMS (Figure 1) includes three separate equipments able to carry out discrete observation and/or continuous monitoring (Stanica and Zugravescu, 2004, Stanica et al, 2004) of: a) HF and LF electromagnetic field (Geophysical Electromagnetic Measurement System - GMS 06, Metronix-Germany); b) Geomagnetic field (MAG 03 DAM, Bartington-England); c) Geoelectric field (Resistivimeter INTEL V3, INTEL92-Romaia).

All the three measurement equipments have specific sensors, data acquisition modules and adequate software.

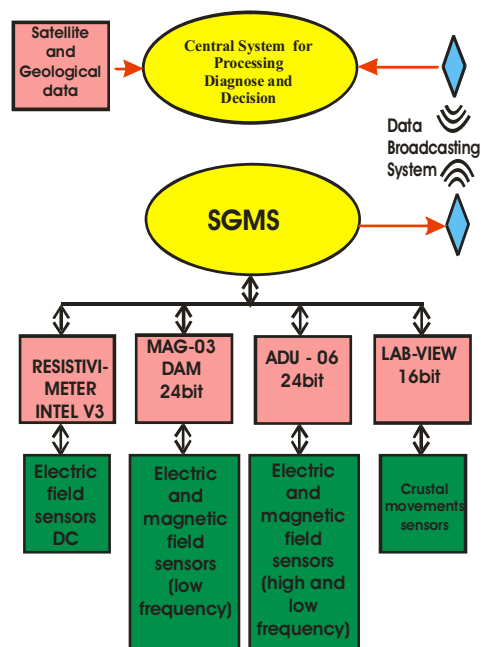


**Figure 1.** Specific ground-based monitoring system (only the electric and EM components have been presented in this paper)

The MAPROS software packages (Metronix-Germany) used for the electromagnetic system runs under Windows 95 or Windows NT operating systems, on a laptop connected to a single ADU or an ADU network. The tasks performed by MAPROS are:

- In-field system calibration and automatic offset compensation;
- Real time data acquisition and processing;
- Robust estimation of transfer functions;
- Real time display of time series and all important EM-parameters;

### METHODOLOGY AND RESULTS

The objectives of the paper are to be focused on the recognition of the electromagnetic parameters which could be correlated with landslide and seismic activity. The studies had to be involved in a multi-parameters context and, therefore in the Provita de Sus - test site we installed the discreet and continuous monitoring systems of the electric, magnetic and EM fields.

The main condition for a specific approach of this problem was to use long time continuous electromagnetic data and appropriate algorithms to extract possible anomalous variations, so that we could make an analysis of the electromagnetic results during

the landslides processes. Thus, the MAPROS software packages and specific methodology have been applied for obtaining, in real time, all the important electromagnetic parameters and to point out the anomalous behaviour versus the specific pattern pre-established in non active-tectonic conditions.

As a first stage in getting to this aim, it is important to mention the specific equipment used for real-time monitoring of the electromagnetic field and the methodology applied to calculate the time evolution of the electromagnetic parameters. By using magnetotelluric (MT) tensor impedance decomposition procedure it was possible to separate the local effects from the regional ones, to identify the type of geological structures and to emphasize the strike orientation of the possible new fractured zones occurred at shallow depths interval.

The selection methodology for precursory EM parameters was established according to the geotectonic features of the Provita de Sus landslide zone. It is also necessary to mention that, according to the frequency range taken into consideration - corresponding to the shallow geodynamic processes, the processing and the analysis of the time series were accomplished in such a manner that these enable to highlight the anomalous fluctuations of the electromagnetic parameters. Subsequently, the specific methodology have consisted in extracting of the peculiar changes in time of the resistivity - parallel and perpendicular to the geological strike, electrical anisotropy, skewness and strike, and to reveal the low frequency electric signals, that "arrive" before the time derivative of the magnetic field, emitted prior the stress reached a critical value.

By analyzing EM data carried out at Provita de Sus (test site), it was possible to connect the increased activity of landslide with the PF reactivation generated by the earthquake of M=6 occurred in the Vrancea zone, on November 27-th, 2004. This earthquake has also been remarked by the anomalous behaviour of the electromagnetic parameter Bzn (Stanica et al., 2004; Stanica et al., 2006) recorded at National Geophysical Observatory Surlari .

The EM field results, which will be presented, reflect the following two activities:

#### a. Experimental studies to establish geoelectric/electromagnetic pattern of the test site in „pre-critical” conditions

All the electromagnetic data, obtained during the experimental studies (Stanica et al., 2006), conveyed to:

- Specific tomographic images carried out by using both the vertical electrical soundings (VES) in Figure 2 and magnetotelluric soundings (MTS) in Figure 3;
- Estimation of the skewness parameter;
- Estimation of the geological strike;

- Assessment of the anisotropy.

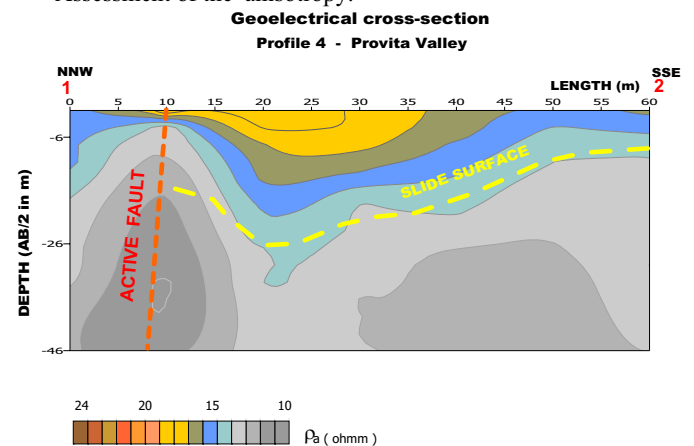


Figure 2. Geoelectric tomography along the VES profile perpendicular to the active fault (PF)

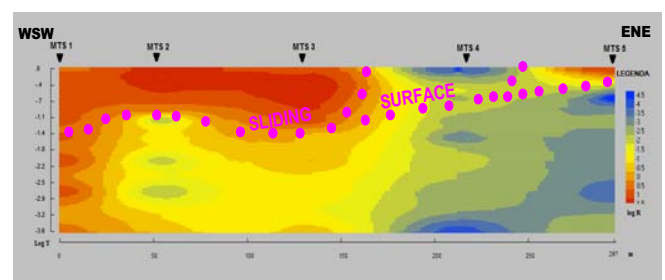


Figure 3. Magnetotelluric tomography (B-polarized mode) along the MTS profile perpendicular to the landslide

#### b. Monitoring of the EM parameters /phenomena related to the landslide activity

In order to determine the time evolution of the slide activity occurred in the Provita de Sus test site, we made the measurements in the same point on landslide (electric and magnetic sensors in unchangeable position), with a sampling rate of 7 days, of both the EM parameters (skewness, strike and anisotropy) and the low frequency electric signals, that "arrive" before the time derivative of the magnetic field, emitted prior the stress reached a critical value.

Further on, some examples regarding this activity are set off:

- Skewness parameter recorded on 30-th September, 2005 and 07-th October, 2005;
- Strike parameter recorded on 30-th September, 2005 and 07-th October, 2005 ;
- Electrical anisotropy recorded on 30-th September, 2005 and 07-th October, 2005 ;

The results reveal the significant changes of the EM parameters as follows:

- In the frequency range  $2.10^3$ -  $4.10^3$  Hz, specific to the sliding activity occurred in the depth interval 0-30m, skewness parameter being higher than 0.3 revealed a 3D structure (for 30-th September), while the same structure becomes 2D on 07-th October (when the skewness is smaller than 0.3);
- For the both records, the strike parameter has deviations of about  $12^0$  versus its mean value ( $92^0 \pm 2^0$ ), which maybe assigned to the main rupturing process of the landslide that could be associated with the sliced blocks having complex array of micro-faults with different orientation;
- In the same frequency ranges  $2.10^3$ -  $4.10^3$  Hz, the electrical anisotropy is of about 1.8 on 30-th September and becomes of about 2.0-2.5 on 07-th October.

As regards the low frequency electric signals emitted prior the stress reached a critical value, we used a special array of electrical sensors having the interval (D) between two pairs of 8m. Such an experiment has success if the interval between the sensors is chosen so that the electrical spike to be not masked by natural electric variations (for D=16m the electrical spike is partially masked by natural electrical field).

### CONCLUSIONS

The described SGMS and methodology proved an effective way of monitoring the EM parameters and phenomena in order to detect their significant changes associated to Provita de Sus landslide. The following general conclusions can be drawn from this test site:

1. In 2005 year, in the Provita de Sus landslide the active fault (PF), reactivated by intermediate depth Vrancea's earthquakes and strong rainfalls were the major forces generating the slide activity. Significant morphological-geo-electrical changes on the landslide surface and its shallow depth (0-20m) had a local character only and were developed mainly between the middle and front part of the landslide. This process deforms the small sliced blocks and produces a complex array of reverse micro-faults, strike-slip micro-faults and folds;
2. The accuracy of the EM parameters' changes versus the geodynamic characteristics of the Provita de Sus landslide allowed us to consider the SGMS as powerful tool to investigate any landslide areas characterized by very complex geology;
3. The related study demonstrates the rich potential of using this new methodology for landslide monitoring. In particular, the SGMS can play an important role in monitoring of landslide-prone areas and in providing, in near real-time, warnings on the slide motions that can put in danger the life and properties;

4. High-resolution of the EM parameters and tomographic images can lead to an improved understanding of landslide mechanism and hazard assessment due to the seismic activity.

### REFERENCES

- HAEBERLIN, Y., TURBERG, P., RETIERE, A., SENEGAS, O., PARRIAUX, A., 2004, Validation of Spot-5 satellite imagery for geological hazard identification and risk assessment for landslides, mud and debris flows in Maragalpa, Nicaragua, the XX-th ISPRS Congress, Commission I papers, vol. XXXV, part B1, Int. Soc. for Photogramm. and Remote Sens., Istanbul, Turkey, 12-13 July.
- MALET, J.P., MAQUAIRE, O., CALAIS, E., 2002, The use of global positioning system techniques for the continuous monitoring of landslides: Application to the Super size Earth flow (Alpes-de-Haute-Provence, France), *Geomorphology*, 43, 33-54.
- McKEAN, J., and ROERING, J., 2004, Objective landslide detection and surface morphology mapping using high-resolution airborne laser altimetry, *Geomorphology*, 57, 331-351.
- MORA, P., BALDI, P., CASULA, G., FABRIS, M., GHIROTI, M., MAZZINI, E., PESCI, A., 2003, Global Positioning System and digital photogrammetry for the monitoring of mass movements: Application to the Ca' di Malta landslide (northern Apennines, Italy), *Eng. Geol.*, 68(1-2), 103-121.
- STĂNICĂ, D., ZUGRĂVESCU, D., 2004, Mobile geophysical laboratory: electromagnetic, electric and seismo-acoustic analysis, *Studi Geologici Camerti*, Special Issue, Active Faults: Analysis processes and monitoring, EDIMOND, Italy, 131-134.
- STANICA, D., STANICA, M., TATU, M., DIACOPOLOS, C., 2005, Geophysical measurement system (GMS) used for real-time monitoring of landslides in active tectonic zones (Provita and Doftana Valleys) Technical Meetings of the INTEGRATED OPTIMIZATION OF LANDSLIDE ALERT SYSTEMS (OASYS)-EU FP5 Project, Modena, Italy, 3-4 February.
- STANICA, M., STANICA, D., DIACOPOLOS, C., 2006, Long term continuous monitoring of the landslides associated with seismic events. EGU, *Geophysical Research Abstracts*, Volume 8, 01803.

## **Geophysical estimation of dissolved apparent porosity and salt loads**

Yusen Ley-Cooper, Monash University, Australia  
James Macnae RMIT University, Australia  
Sarah Tweed Monash University, Australia

---

### **SUMMARY**

Based on Archie's law, we have fused geophysical conductivity sections with hydro-geological depth EC data to map apparent porosity and predict dissolved salt loads. This exercise provides the disciplines involved in the modelling of ground water with a powerful physical measurement methodology. Interpolated electrical conductivity, sampled at the water table in sparsely distributed boreholes, can be combined with bulk conductivities estimated from airborne electromagnetics to provide a detailed prediction of subsurface porosity and total dissolved salt load

The process has been applied to the saturated zone in the Honeysuckle Creek area of Victoria, Australia. Iconic location for salinity related studies. Multidisciplinary consensus on the interpretation of data has not been reached; with alternative conclusions that measured borehole electrical conductivities (EC), do or do not relate to airborne electromagnetic (AEM) conductivity values

**Keywords:** Airborne Electromagnetics Salinity Porosity

---

### **INTRODUCTION**

Groundwater is a resource of increasing value. Rising salinity has reduced agricultural viability, and is perceived as a threat in others. To address the problem of land and water salinisation intelligent action requires knowledge and accurate understanding of the subsurface distribution and migration of saline water in the host environment.

Hydrogeologists traditionally have made subsurface predictions based on sets of data measured from boreholes, and stream observations. These on-ground investigations provide valuable information on the in-situ properties of the groundwater and soil characteristics. However, drilling and logging boreholes is both expensive and limited by access issues, which usually lead to sparse data. To interpret processes occurring in the subsurface, a more thorough spatial distribution of hydrogeological data is required.

Boreholes can be logged geophysically to provide reference samples of bulk EC as a function of depth and can independently sample fluids seeping from the

borehole walls to derive water EC as well. The relationship between bulk and fluid EC is complex, but has been approximated by expressions such as Archie's law.

Extended coverage geophysical techniques can therefore potentially delimit an aquifer's extensions and geometry; define hydraulic properties (porosity, clay content), determine quality of the water (salty, fresh, and contaminated) and monitor water flow.

Geophysicists have used AEM to map bulk conductivity as a function of depth. Papers in the recent literature have found it difficult to reconcile the geophysical bulk EC, conventionally presented in maps with a constant depth below surface, and the hydrogeological data (Christensen, 2003; Cresswell et al., 2004). With several major simplifying assumptions, we justify in this paper how a combination of point sampled fluid electrical conductivities EC's, water table depths and AEM bulk EC's can be used to predict distribution of apparent porosity and dissolved salt loads.

## HYDROGEOLOGICAL AND PHYSICAL PROPERTY SAMPLING

In the Honeysuckle creek area, a  $2400 \text{ km}^2$  study region well known in Australia for salinity problems, data from 241 boreholes were available (English et al., 2004). Within  $1194 \text{ km}^2$  of that region, data from a government AEM survey was also on hand. A linearly interpolated conductivity map of groundwater EC, as sampled at the top of the watertable is shown in Figure 1. The imaged EC map has been confined to the airborne survey area; with bores shown by crosses with a surrounding red circle. Note the irregular spatial sampling of data, with some areas many km from the nearest borehole.

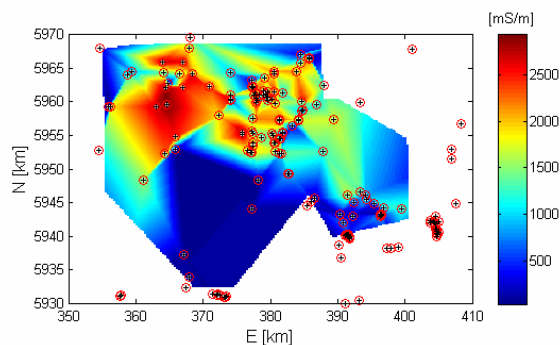


**Figure 1** Map of EC values at water table depth, linearly interpolated from 241 boreholes within and surrounding the Honeysuckle area. Note the irregular spatial sampling, with some areas many km from the nearest borehole. The imaged EC's are confined to the area of the airborne survey. This map does not consider temporal variation, just spatial variation of the dataset

These bores provide important hydrogeological information of the area like water table depths and conductivity values. High EC values have been associated with elevated concentrations of total dissolved solids. In the northern region where conductivities are high, the horizontal hydraulic gradients are low ( $\sim 0.001$ ).

## AIRBORNE ELECTRO MAGNETICS

The airborne electromagnetic data was acquired with the Tempest system, a fixed wing airborne system sampling in the time domain. This data has been transformed to conductivity as a function of depth. Several techniques and interpretations of this area have resulted in the publications of a number of papers (Cresswell et al., 2004; Philips and Ely, 2002), and government reports (English et al., 2004; Spies and

Woodgate, 2005) However, while hydrogeology and AEM data sets have been compared and the use of AEM as a mapping tool has been acknowledged, no analysis to date appears to have attempted to quantitatively integrate the borehole and airborne measurements of EC.

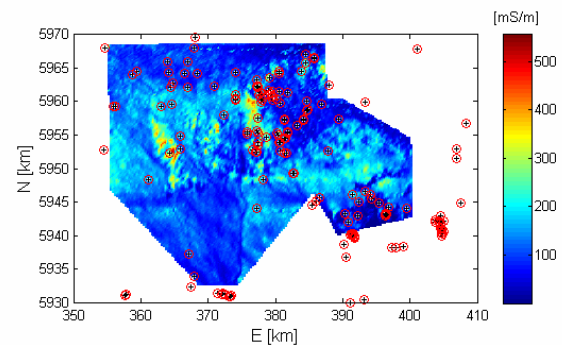


**Figure 2** Spatially detailed electrical conductivity EC data derived from airborne EM data for a slice from 0 to 5 meters below surface. AEM data was sampled at about 10 m spacings along lines spaced 200 m apart

Figure 2, shows estimates of conductivity averaged from surface to a five meter depth as derived from the airborne electromagnetic data. A logical assumption might be to correlate both data sets shown in Figures 1 and 2, since; both reflect conductivity values (in mS/m). Clearly the spatial distributions are different. Further, borehole conductivities vary up to 3000 mS/m while airborne is limited to 400mS/m.

## BULK AND FLUID CONDUCTIVITY

A recent review by (Guérin, 2005) describes the hydrogeological properties of relevance in salinity studies; these being in particular porosity, hydraulic permeability, water, salt and clay content. An association between these parameters and geophysical data can only be attempted through physical parameters associated with each property. One such physical parameter, bulk electrical conductivity depends on salinity, water saturation, porosity, the presence of conductive solids and also on temperature which affects conductivity at constant salinity.

Other than clays, most common constituent minerals making up the earth are electrically resistive. For a matrix of electrically resistive minerals saturated with a saline fluid, the bulk conductivity can be calculated by Archie's relationship Equation 1

$$\text{Equation 1 } \sigma_r = a^{-1} \phi^n \sigma_w$$

where  $\sigma_r$  and  $\sigma_w$  are saturated-bulk and water conductivities respectively,  $\phi$  is porosity, while  $a$  and  $n$  are empirical constants. This equation states that saturated and saturant solution resistivities have a linear dependency with a constant factor (sometimes called the formation factor) which is an inverse function of porosity.

As water saturation  $S_w$  decreases, bulk conductivities also decrease with an approximate relation of:

$$\text{Equation 2 } \sigma = S_w^n$$

AEM data can be inverted to provide spatially averaged estimates of bulk conductivity  $\sigma_r$  as a function of depth, which can potentially be related to porosity and water resistivity through equation 1.

The presence of clays adds complexity in defining a predicted bulk conductivity value, since clay minerals bind water to their surfaces and are electrically conductive. Even when clays have low water contents, their resistivities depend on the salinity of the bound water. (Emerson and Yang, 1997), showed however that whether we consider clays or other minerals, the more saline the volume, the more conductive the bulk becomes.

### The saturated and Vadose zones

We can crudely categorise the earth into two main hydrostratigraphic structures; the saturated volume at depth and a shallower unsaturated or vadose zone. A profile in Figure 3, shows a section along one of the airborne survey lines, with depths to water as interpolated from boreholes. This saturated zone is the region where Archie's law can be expected to apply in the form given above.

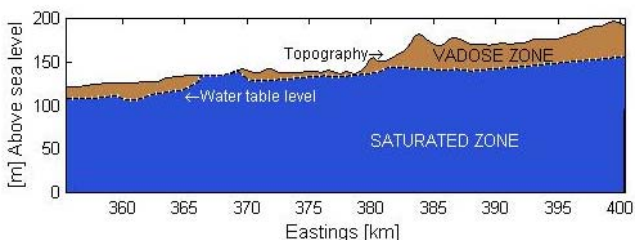


**Figure 3** Section beneath a line of airborne EM, using depths interpolated from boreholes to define the water table.

Bulk conductivity estimates from the airborne EM data, predicted at the interpolated depth of the water table are imaged in Figure 4. Again, the bulk conductivities are significantly less than the sampled water conductivity imaged in Figure 1. This image is clearly superior in detail and in the information that can be extracted from it that those presented in Figures 1 or 2.

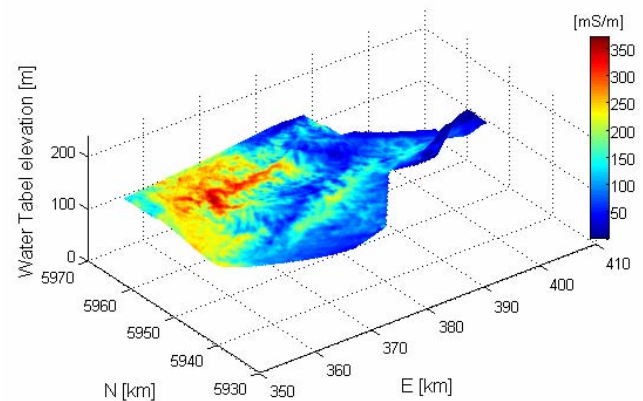


**Figure 4** Map of airborne bulk conductivity estimates at the top of the water table, plotted on a drape showing the interpolated elevation of the water table itself.

### POROSITY PREDICTION FROM EC AND AEM

In order to use equation 1 to predict porosity we need to make three sweeping assumptions. First, we assume that the conductivity of water sampled at the top of the watertable from (shallow) boreholes is typical of waters at greater depth. Secondly, we assume that salinity and depth to water table is reasonably spatially consistent so that simple linear interpolation of the sparse borehole values is warranted. This interpolated borehole data defines the saturated zone as shown in the profile (Figure 3.). Thirdly, we will assume that porosity in the saturated zone is constant up to some greater depth. Porosities predicted by substitution into equation 1 with these three additional assumptions will be called apparent porosity, and give the symbol  $\phi_a$ . For convenience we have chosen 80 m, well within the depth capability of the AEM system as the maximum depth. In practice, porosity is likely to decrease with increasing depth.

Using interpolated water conductivity from boreholes and the spatially detailed bulk conductivity in the saturated zone as derived from AEM, we predict an apparent porosity  $\phi_a$ . using assumed values for  $a$  and  $n$ , (Elliott and Thomas, 1986) gave empirical values of  $a = 0.81$  and  $n = 2$  for clean sands, and  $a = 1$  and  $n = 1.4$  for unconsolidated sediments. We used an average of these values in our calculations. Because of the assumption of a resistive solids matrix in Archie's law,

the apparent porosity calculated by equation 1 is in fact an upper limit porosity, where the host matrix is conductive (as is the case for clay minerals), apparent porosities calculated will be too large.

Airborne EM was used to estimate the bulk conductivity values at different depths, in order to calculate maximum porosity we need to choose that part of the Airborne EM conductivity values that lie within the saturated zone. The borehole information determined the depth below which Airborne EM conductivities would be used; they determined a location, with its depth to water and EM value of this water.

Widely accepted porosity values are available in the literature (McWorter and Sunada, 1977) from which we have accepted 40 percent as a maximum credible value. The map of predicted maximum porosity is shown in Figure 5.

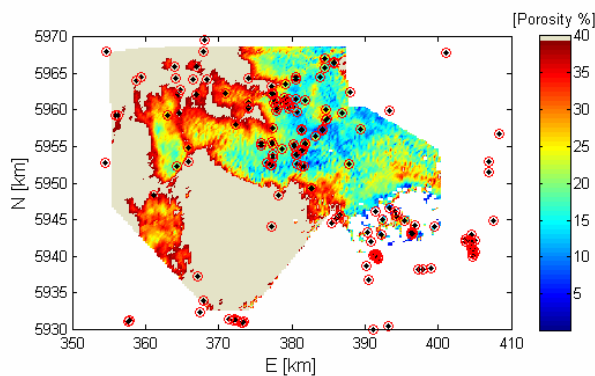


**Figure 5** Apparent porosity calculated for the saturated zone. Values exceeding 40% are blanked, and are likely to indicate significant clay concentrations. Uses all aballabel bores regardless of depth the (all in the saturated zone)

**SALT LOAD PREDICTION FOR SATURATED ZONE**

Water salinity can be defined as a measured of concentration of dissolved solids in proportion to the amount of solvent, in this, case groundwater. In accordance with the characteristics of the study area, we have quantified the salt load in tones per hectare.

In (McNeill, 1997) the relation between fluid conductivity and total dissolved solids (TDS) is given by:

$$\text{Equation 3 } TDS = 6\sigma$$

This empirically relates the EC of groundwater measured from bores (in S/m) to total dissolved solids (expressed as a fraction of the total volume of groundwater).

Hence, the salt load per unit of area to a depth of interest d can be calculated by the product:

$$\text{Equation 4 } D \cdot \phi \cdot TDS \cdot \rho,$$

where D is depth from the top of the water table down to the depth of interest d and  $\rho$  is the density of water. An average TDS is derived from an average of the conductivity in the saturated zone down to depth d.

Figure 6 plots total salt load as estimated from equations 3 and 4. Since apparent porosities arte likely to overestimate true porosities, this map is likely to overestimate than underestimate the dissolved salt load. The total magnetic field enhances the shallow geological features of the data; it is very interesting to note how the apparent salt load seems to accumulate in the underling paleo-channels, which are often natural reservoirs containing sands and gravels.

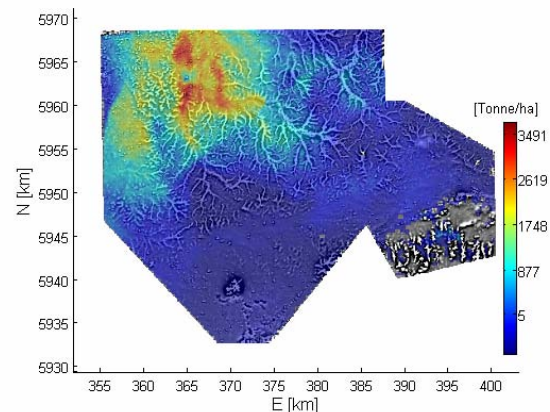


**Figure 6:** Map of dissolved maximum salt load, expressed in tonnes per hectare, up to a depth of 80 m below the surface. Shading is derived from a first-vertical-derivative total field magnetic map shows palaeochannel drainage patterns.

**EXTENSIONS OF THE METHOD: DEEP CONDUCTIVITY, THE VADOSE ZONE AND CLAY CONSIDERATIONS**

Porosity and hydraulic permeability tend to decrease with increasing depth due to compression, so an obvious extension would be to estimate porosity in

depth slices rather than as an averaged property up to a depth of interest as presented here. For this purpose, it would be of benefit also to have bores that sampled groundwaters to greater depths. It would also be worthwhile to log bores to measure porosities for comparison with our predictions. Detection of clay rich zones in boreholes might usefully constrain layers to excise from the dissolved salt calculation.

In the drier parts of the vadose zone, well above the water table, high conductivities can not be due to free saline water, but must be attributed to an alternative source such as bound water in clays. Commonly, the effects of culture on the EM data, such as grounded fences and powerlines, can produce conductive features in the section that are not of geological or hydrological origin.

Conductors deeper in the vadose zone are likely to correspond to either or both of clays and partially saturated saline waters. However, broad assumptions as to the degree of saturation are required to derive estimates of porosity or salt load for this shallower volume of the section, and we have not undertaken this as a result.

#### APPLICATIONS

The mapped distribution of apparent porosity values, particularly in such a complex system comprising both fractured and porous mediums across multiple aquifer lithologies, provides valuable information for (i) hydrogeological modeling, and (ii) spatial distribution of salt loads for water and land resource management. Defining the 3-D sub-surface distribution of hydraulic parameters for groundwater numerical models is often limited by the spatial resolution of the bore network. The porosity maps generated highlight an increase in apparent porosity values with depth in the fractured bedrock aquifer, and an increase in apparent porosity values in the shallow alluvial aquifer compared with the fractured bedrock aquifer. The shallow salt load map indicates that the alluvial aquifer in the northwest has the greatest salt load. However, the rate of migration of this saline groundwater, as it flows northwest, requires information on the hydraulic permeability within the clay-rich shallow aquifer.

#### CONCLUSIONS

Provided that interpolation of sparse borehole data gives reasonable estimates of water EC values, depth to the water table and the groundwater EC, where clay content is minimal and where porosity does not vary significantly with depth, detailed AEM data can provide a detailed map of apparent porosity of the saturated zone. Since the calculation assumes that electrically resistive minerals host the saline water, the apparent porosity calculated will tend to be a maximum

porosity. Values of apparent porosity exceeding 40% are likely to indicate the presence of electrically conductive clays forming the host matrix and a much lower true porosity.

Using established empirical relationships between total dissolved solids and electrical conductivity, the maximum dissolved salt load can then be calculated. This calculation can be performed for the zone beneath the water table and up to the penetration depth of the AEM system.

An area with high porosity and elevated concentrations of salt, where ground water levels are close to surface is a potential hazard, which may cause social, economic and environmental degradation. Identifying these areas through the methodology proposed here may prove to be very useful to the general community.

#### ACKNOWLEDGEMENTS

The Department of Primary industries Victoria for letting us have access to the airborne data

Pauline English (CSIRO Land and Water) for letting access the borehole data, and contributions from Tamie Weaver (University of Melbourne).

#### REFERENCES

- Christensen, A., 2003, Calibration of Honeysuckle Creek Conductivity Depth Imaging: Preview Bulletin of Exploration Geophysics, v. 106.
- Cresswell, R. G., D. L. Dent, G. L. Jones, and D. S. Galloway, 2004, Three-dimensional mapping of salt stores in the southeast Murray-Darling Basin, Australia. 1. Steps in calibration of airborne electromagnetic surveys: Soil Use and Management, v. 20, p. 133-143.
- Elliott, P. J., and L. T. Thomas, 1986, Interpretation of lithology from the formation resistivity of unconsolidated argillaceous/arenaceous sediments: Exploration Geophysics, v. 17 (2), p. 75-79.
- Emerson, D. W., and Y. P. Yang, 1997, Effects of Water Salinity and Saturation on the Electrical Resistivity of Clays: Preview Bulletin of Exploration Geophysics, v. 68, p. 19-23.
- English, P., P. Richardson, M. Glover, H. Cresswell, and J. Gallant, 2004, Interpreting Airborne Geophysics as an adjunct to Hydrogeological Investigations for Salinity Management: Honeysuckle Creek Catchment, in CSIRO, ed., Land and Water Technical Report, Victoria., CSIRO.

Guérin, R., 2005, Borehole and surface-based hydrogeophysics.: Hydrogeology Journal, v. 13.

McNeill, J. D., 1997, use of electromagnetic methods for ground water studies, in S. H. Ward, ed., Geotechnical and environmental Geophysics, v. I: Tulsa, Oklahoma, Society of Exploration Geophysicists, p. 191-219.

McWorter, D. B., and D. K. Sunada, 1977, Groundwater Hydrology and Hydraulics, Water Resources Publications: Ft. Collins Colorado.

Philips, G. N., and K. S. Ely, 2002, Victoria Undercover Conference Proceedings and Field Guide: Victoria Undercover.

Spies, B., and P. Woodgate, 2005, Salinity Mapping Methods in the Australian Context, Prepared for the Natural Resource Management Ministerial Council Department of the Environment and Heritage and Department of Agriculture, Fisheries and Forestry.

## **On the first field data of a new radiomagnetotelluric device operating in the frequency range from 10 kHz to 1 MHz**

B. Tezkan, University of Cologne, Institute for Geophysics and Meteorology, Cologne, Germany  
A. Saraev, St. Petersburg State University, Earth Crust Institute, St. Petersburg, Russia  
V. Schuman, Academy of Science of Ukraine, Institute of Geophysics, Kiev, Ukraine  
P. Georgescu, University of Bucharest, Faculty of Geology and Geophysics, Bucharest, Romania  
N. B. Christensen, University of Aarhus, Department of Earth Sciences, Aarhus, Denmark

---

### **SUMMARY**

A new radiomagnetotelluric (RMT) device was developed which can record time series of electric and magnetic fields in a wide frequency range of 10 kHz to 1 MHz. Transfer functions were determined by spectral analysis using a newly developed processing software. A workbench program was developed in which the transfer functions were interpreted by conductivity models based on new inversion algorithms.

The developed tensor radiomagnetotelluric device was tested in the laboratory and then applied successfully in the field on several environmental and groundwater problems in Russia, Ukraine, Denmark, Romania, and Germany.

The observed transfer functions in the field are the first ones in the frequency range above 300 kHz which can lead to a better resolution of the shallow structure. The new device enables quick and efficient mappings of polluted areas and tensor measurements allowing a 2D or 3D interpretation of the field data.

Transfer functions and their 2D inversions will be shown from the field surveys in Russia and Ukraine as representative examples. RMT measurements in St. Petersburg/Russia were carried out for the determination of slag thickness and in Uzin/Ukraine for mapping of kerosene contaminations close to a military area.

**Keywords:** radiomagnetotellurics, new device, first field data, 2D modeling

---

### **INTRODUCTION**

The radiomagnetotelluric (RMT) method is one of the newest and innovative methods of applied geophysics. Military and civilian radiostations broadcasting in a frequency range between 10 kHz and 1 MHz are used as transmitters (Bastani 2001, Linde and Petersen 2004, Tezkan et al. 2005). The electromagnetic waves radiated from these transmitters diffuse in the conductive earth and induce current systems which are connected with electrical and magnetic alternative fields. These fields are measured by magnetic and electric antennae for several selected frequencies. Information about the conductivity distribution of the earth can be derived from 1 meter to 100 meter downwards.

The main objective of this study was to develop a new radiomagnetotelluric (RMT) device and a new interpretation software for the modelling of RMT field

data. The measurements with the new device should enable quick and efficient mappings and soundings of the shallow earth structure (e.g. localisation of contamination, waste site exploration, groundwater, geomorphology...). Quick data processing and interpretation should be possible with the new interpretation software. Finally, the device should be applied on real field cases. The main aim was to observe reliable data in the frequency range between 10 kHz and 1 MHz which could be interpreted by conductivity models.

### **THE NEW DEVICE**

The RMT-system consists of a digital recorder, electrical and magnetic antenna. The recorder is intended for the transformation of analogue signals coming from two magnetic and electric antennae into digital codes of data acquisition. The signal is primarily processed in the recorder and saved in digital form.

The electrical antenna is represented by a symmetrical electrical dipole. The output of the electrical antenna is connected with differential input of the preamplifier. The magnetic antenna is represented by a cylinder of about 30 cm length with a multi section coil in the centre of which is a core of high permeability. The digital recorder is shown in Fig. 1.



**Figure 1.** The new digital RMT receiver.

Two different measuring modes (time series and spectral mode) are implemented in the device. The RMT-F device works with two frequency bands: D2 band (10 kHz - 100 kHz,  $\Delta f = 312.5$  kHz) and D4 band (100 kHz - 1 MHz,  $\Delta f = 2.5$  MHz) whereas the RMT-M device operates between 10 kHz and 300 kHz. The electric and magnetic field values are registered simultaneously. The user can select the gain factor, the

frequency range, segment length etc. using the software in the device.

The RMT time series are transferred via Ethernet cable and processed with a new developed software on a PC. Thus the observed time series of any selected station can be visualized, and auto and cross spectra can be calculated and displayed. Additionally, the coherency between the electric and magnetic fields oriented perpendicular to each other is also calculated and displayed. The user can define a coherency level (e.g. 0.8) and then only frequencies of coherencies greater than this level are used to calculate the transfer functions. Fig. 2 shows an example of an auto spectrum from time series of electric and magnetic field components in the frequency range of 10-100 kHz (D2 band).

A similar presentation is easily obtained for the D4 band. A quick estimation about the signal/noise ratio of the investigated area is possible if such a type of displaying the data is used. This is even possible in the field. Another possibility is the visualization of azimuths of existing radio transmitters.

All the azimuths of the radio transmitters available in the survey area can be viewed by the software in the frequency band 10 kHz - 100 kHz or in the frequency band 100 kHz - 1 MHz. The azimuth is calculated relatively to the magnetic field in the north direction, and the user can define an azimuth range in which to select the available transmitters. The coherency level, typically with a value of 0.8, can be selected in the program by the user. Thus, the transfer functions need only to be calculated for the frequencies with coherencies greater than the selected coherency level

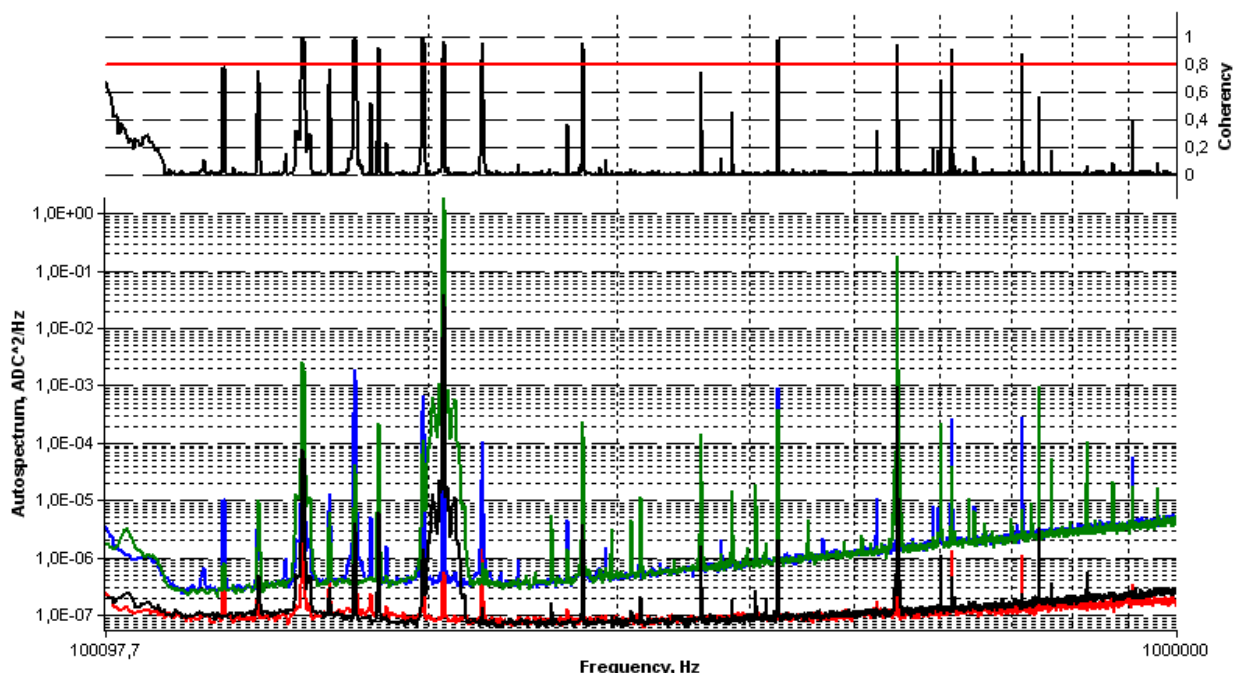


**Figure 2.** Auto spectra calculated from time series in the frequency range of 10 - 100 kHz.

and for radio transmitters located within the azimuth range defined by the user.

After having calculated the power and cross spectra and after having determined the coherencies and azimuth angles, transfer functions (apparent resistivity and phase) are derived for each frequency from the power and cross spectra.

### CASE STUDY IN ST. PETERSBURG, RUSSIA

The survey area is located in the south eastern part of St. Petersburg (Fig. 3 and 4).

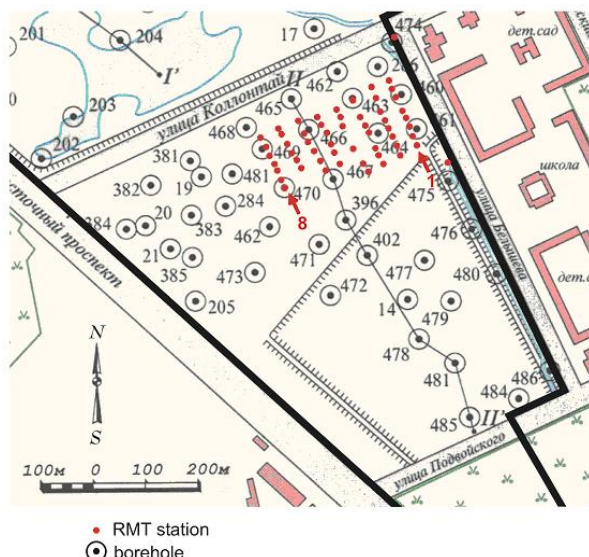


**Figure 3.** Sketch of the survey area in St. Petersburg.

Some years ago, the Russian railway company used the area as a slag heap. The aim of the measurements was to find out if the lower boundary of the slag can be mapped with the RMT method. According to borehole information, the lower boundary of the slag is located at a depth of 1-5 m. There is a clay layer beneath it extending to about 12 m. At each station time series in the frequency range between 10 kHz – 1 MHz were recorded with the new RMT-F device.

The apparent resistivity, the phase, and the transmitter direction were calculated automatically if the coherency between the magnetic and the perpendicular electric field was bigger than 0.8. Fig. 5 shows a data example of the first profile in Fig. 3.

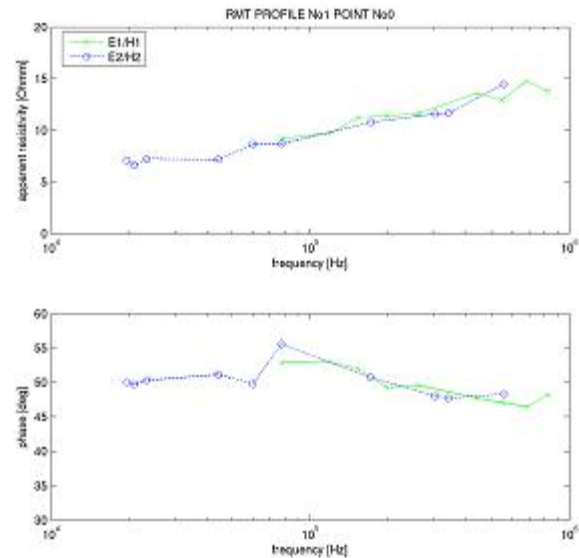


**Figure 5.** Apparent resistivity (top) and phase (bottom) versus frequency for the direction of transmitters in profile direction (green) and perpendicular to the profile direction (blue). Frequencies up to 1 MHz were recorded.

The data are smooth and reliable. Fig. 6 shows the 2D inversion results for profile 1, as a representative example for the inversion of all profiles. The inversion calculations were carried out using the algorithm of Mackie et al. (1997). The slag could be resolved as a resistive structure above a clay layer. Similar structures were obtained for all profiles.

### CONCLUSIONS

- A new tensor radiomagnetotelluric (RMT) device has been developed
- Time series of electric and magnetic fields can be recorded by the new device
- Transfer functions can be determined by spectral analysis using a newly developed software
- The transfer functions can be interpreted with



**Figure 4.** Panoramic view of the survey area.

conductivity models based on new inversion techniques

- The observed transfer functions in the field are the first in the frequency range above 300 kHz and can lead to a better resolution of the shallow structure
- The developed RMT technology can be applied to environmental problems (contamination, waste site...) and groundwater exploration

#### ACKNOWLEDGEMENTS

This work was carried out in the framework of the INCO: International Scientific Cooperation Projects financed by the European Union (contact number: ICA2-CT-200-10055).

#### REFERENCES

Bastani, M., 2001, EnviroMT- a new controlled source/radio magnetotelluric system, PhD dissertation, Uppsala Univ., Uppsala, Sweden.

Linde, N., and L. B. Pedersen, 2004, Characterization of a fractured granite using radio magnetotelluric (RMT) data, *Geophysics*, 69, 1155-1165.

Mackie, R., Rieven, S., and Rodi, W., 1997, Users Manual and Software Documentation for Two-Dimensional Inversion of Magnetotelluric data: Massachusetts Institute of Technology, Earth Resources Laboratory, Cambridge, Massachusetts 02139.

Tezkan B., Georgescu, P., and Fauzi, U., 2005, A radiomagnetotelluric survey on an oil-contaminated area near the Brazi Refinery, Romania, *Geophys. Prosp.*, 53, 311-323.

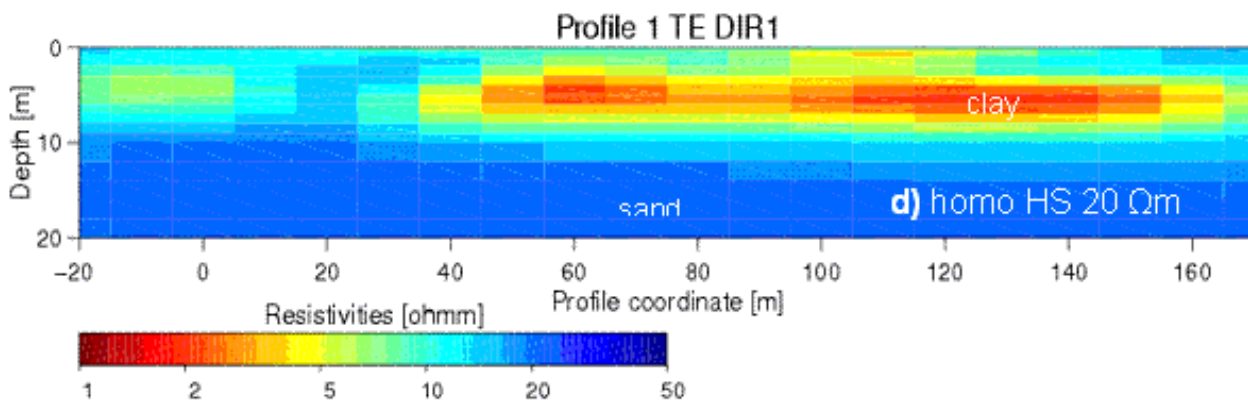


Figure 6. 2D inversion. Start model: homogeneous halfspace with 20  $\Omega\text{m}$ .

---

## Environmental assessment of the Amchitka Island Nuclear Test site (Alaska) with magnetotelluric data

Martyn Unsworth, Department of Physics, University of Alberta, Edmonton, Canada  
Wolfgang Soyer, Geosystem SRL, Milano, Italy  
Volkan Tuncer, Department of Physics, University of Alberta, Edmonton, Canada

---

### SUMMARY

Amchitka Island, in the Aleutian Islands of Alaska, was used for the underground testing of nuclear weapons from 1965 to 1971. Since the test program concluded, there have been concerns about the release of radionuclides into the marine environment. The hydrogeology of small islands such as Amchitka is characterized by a layer of freshwater overlying a saltwater layer. Hydrogeological modelling has provided estimates of the timing and quantities of radionuclides that could be released from the test sites on Amchitka Island but only limited geophysical and well log data are available to constrain these models.

Magnetotelluric (MT) data were collected on Amchitka Island during an expedition in 2004 to give information about subsurface porosity and salinity. MT data were recorded on profiles passing through the Long Shot, Milrow and Cannikin explosion sites. Two-dimensional models of subsurface electrical resistivity were derived and showed a pattern of increasing, decreasing and increasing resistivity with depth at each test site. The depth at which resistivity begins to decrease corresponds to the top of the transition zone as the salinity increases. The deeper increase in resistivity approximates the base of the transition zone (TZ), as salinity remains constant and the decreasing porosity causes a rise in resistivity. The depths of the transition zone were derived as follows: Milrow (900-1700 m), Long Shot (600 – 1700 m) and Cannikin (900-2500 m). Uncertainties in these depths were derived by studying the range of resistivity models consistent with the MT data. Subject to the limits of the analysis, it appears that each of the cavities resulting from underground nuclear explosions were located in the transition zone from fresh to saltwater. This implies shorter transit times to the marine environment than if the explosions had been located in the saltwater layer.

**Keywords:** Underground nuclear testing, environmental geophysics, magnetotellurics, hydrogeology, porosity

---

### INTRODUCTION

Amchitka Island in the western Aleutian Islands of Alaska was used from 1965-1971 as an underground test site for nuclear weapons that were too large for the Nevada test site. Projects Long Shot, Milrow and Cannikin exploded warheads with yields of 0.08, 1 and 5 megatons respectively. Since the test program was concluded, there have been concerns about the transportation of radionuclides into the marine environment. The hydrogeology of Amchitka Island is characterized by a fresh water layer that is recharged from precipitation, and discharges offshore. Flow in the freshwater layer can be quite rapid, while the underlying saltwater layer is relatively stagnant. It is vital to know the hydrogeological context of the underground explosions, since this controls the timing of radionuclide transport into the ocean, which is important for both native and commercial fisheries.



**Figure 1.** Amchitka Island MT survey. Yellow triangles denote the locations of the underground nuclear explosions. Black circles show MT stations recorded in 2004.

A number of hydrogeological studies were made prior to the test program (*US Army Corp of Engineers and USGS, 1965*). Hydrogeological modelling has been used to estimate transit times from the explosion cavities to the marine environment (*Wheatcraft, 1995; Hassan et al., 2002*), and give a wide range of times. Without geophysical constraints on subsurface structure, the uncertainty in transit times remains large. Since 1995, there has been a concerted effort to evaluate and remediate sites in the United States that were contaminated during the production and testing of nuclear weapons. Some of this work has been undertaken through the Consortium for Risk Evaluation through Stakeholder Participation (CRESP). In 2004 a CRESP expedition visited Amchitka Island and undertook a multidisciplinary evaluation of the environment. This included an onshore magnetotelluric (MT) survey that was used to study the subsurface porosity and salinity structure. In this abstract, the MT data are described and the interpretation is outlined.

#### DATA COLLECTION AND PROCESSING

Broadband magnetotelluric data were collected at 29 stations on Amchitka Island in June 2004 using six Phoenix Geophysics V5-2000 systems (Figure 1). Where logistically possible, both electric and magnetic field data were recorded. At sites far from roads, just electric field data were recorded and the magnetic fields from the nearest 5-channel station was used in the data processing. Remote reference processing was essential to remove the noise generated by strong winds. The geoelectric strike direction was computed using the phase tensor method of *Caldwell et al, (2004)*. At high frequency (1000-10 Hz) the MT data were approximately 1-D. Below 10 Hz, a well defined strike of N55°W was observed, parallel to the axis of the island. From 100-0.1 Hz a subtle pattern of high and low apparent resistivity was observed. This indicated the presence of conductive-resistive-conductive-resistive layers with increasing depth. The MT data were then inverted using the algorithm of *Rodi and Mackie (2001)*. Interpretation of MT data from a coastal environment requires that the low resistivity of the seawater is correctly modelled since the seawater is a strong conductor. A resistivity model was developed with a 100  $\Omega\text{m}$  seafloor and simplified bathymetry. Two methods were used to include the conductive ocean in the inversion process. In the first, the resistivity of the seawater and the uppermost seafloor was fixed during the inversion. Inverting for the smoothest model, was found to be unstable and resulted in a spatially rough resistivity model beneath the island. This occurs because any inaccuracy in seawater depth cannot be overcome by extending the seawater conductor to depth, and the inversion placed artificial conductors beneath the island. Fixing just the ocean in this approach resulted in high conductivities

beneath the ocean as a result of smoothing. A more satisfactory approach was to use a softer constraint that allowed the regularization to find the smoothest model compared to the starting model. A wide range of inversions were performed to determine the range of resistivity models consistent with the measured MT data. Representative models are shown in Figure 2. These models were verified through comparison with well log data and synthetic inversion studies. Three-dimensional (3-D) MT modelling was used to show that 3-D induction effects would only be expected below a frequency of 0.03 Hz. Since the quasi-layered structure is imaged by data above this frequency, a full 3-D inversion is not required.

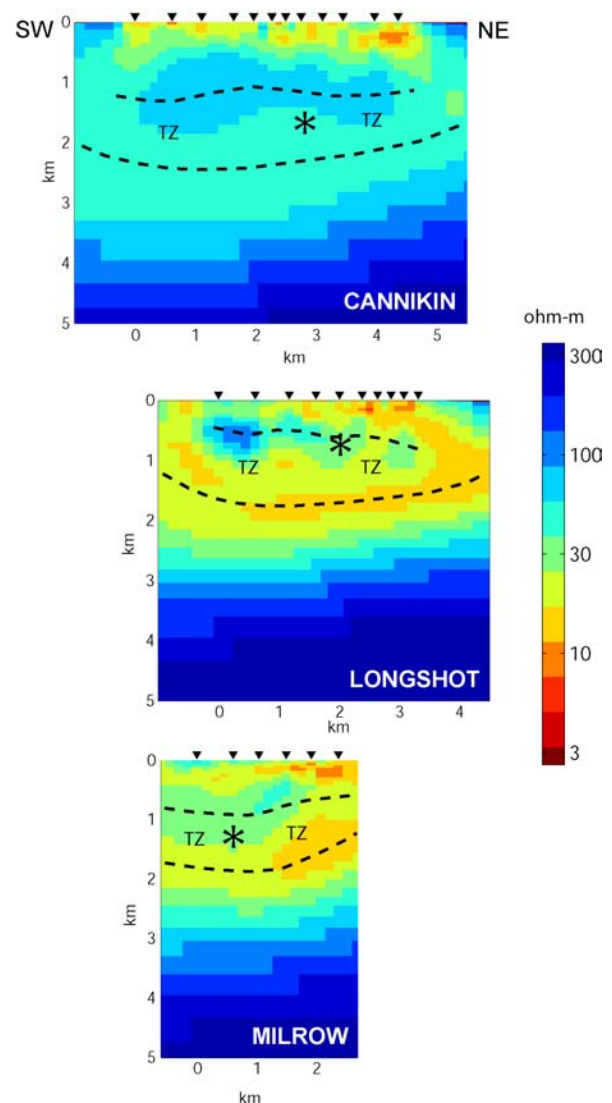


**Figure 2.** Inversion models with asterisks showing the locations of explosions. The dashed lines denote the inferred location of the transition zone (TZ), defined by the downward decrease in resistivity. Trade-off parameter,  $\tau=3$ ; Vertical to horizontal smoothness control parameter,  $\alpha=1$ .

## HYDROGEOLOGICAL INTERPRETATION

Each model shows a four layer structure beneath the island. This can be interpreted using the borehole data collected on Amchitka Island.

- (1) The low resistivity surface layer (0-500 m) corresponds to a zone of relatively high porosity and low salinity (fresh water).
- (2) A layer with increasing resistivity that is caused by decreasing porosity within the fresh water layer (500-1000 m).
- (3) A layer of decreasing resistivity caused by an increase in salinity as the saltwater layer is encountered. This layer represents the transition zone (TZ) from fresh to saltwater and the depth varies from profile to profile.
- (4) The lowest layer shows an increasing resistivity and is produced by a constant salinity within the saltwater layer and a decreasing porosity.

The depths of the transition zone were derived from the resistivity model as follows. Milrow (900–1700 m), Long Shot (600–1700 m) and Cannikin (900–2500 m). Uncertainties in these depths were derived from the range of inversion models consistent with the MT data. Subject to the limits of the data analysis, it appears that each of the cavities resulting from underground nuclear explosions are located in the transition zone from fresh to saltwater. This implies shorter transit times to the marine environment than if the explosions had been located in the saltwater layer.

This analysis was extended to determine combinations of porosity and salinity that were consistent with the resistivity depth profile determined with the MT data. A porosity-depth variation was computed for the Milrow site using Archie's Law (Archie, 1942) and an empirical relationship between salinity and ground water resistivity (Block *et al.*, 2001; Figure 3). Similar porosity-depth variations were derived for the Long Shot and Cannikin locations (Figure 4). These porosity-depth variations are consistent with global compilations of porosity-depth variations (Giles *et al.*, 1998). These porosity values and transition zone depths are being used in hydrogeological modelling to predict the transit time for the transport of radionuclides from the explosion cavities to the Bering Sea and Pacific Ocean (Wagner *et al.*, 2006).

## ACKNOWLEDGEMENTS

This report was prepared with the support of the U.S. Department of Energy, under Award No. DE-FG26-

00NT40938 to the Institute for Responsible Management, CRESP-II. Any opinions, findings, conclusions, or recommendations expressed herein are those of the authors and do not necessarily reflect the views of the Dept. of Energy. The 2004 field work was made possible by Anna Wagner, Chrystal Rae William Shulba and Dan Volz (Expedition Manager). Logistical support from B+N Fisheries and the crew of the F/V Ocean Explorer is also gratefully acknowledged. Technical support from Phoenix Geophysics resulted in the high quality MT data. Bathymetry data were provided by R. Aguirre, Z. Kowalik, and M. Johnson. The authors acknowledge discussions with Anna Wagner, Dave Barnes, Ben Rostron, Carl Mendoza, David Kosson, and Chuck Powers.

## REFERENCES

- Archie, G. E., 1942, The electrical resistivity log as an aid in determining some reservoir characteristics, Transactions American Institute of Mineral. Metallic and Petroleum Engineers, 146, 54-62.
- Block, D., 2001, Water Resistivity Atlas of Western Canada Abstract, at Rock the Foundation Convention of Canadian Society of Petroleum Geologists, Calgary, June 18-22.
- Caldwell, T.G., H. M. Bibby and C. Brown, 2004, The magnetotelluric phase tensor, Geophysical Journal International, 158, 457-469.
- Giles, M.R., S.L. Indrelid and D. James, 1998, Compaction – the great unknown in basin modeling, in Duppenbecker, S.J. and J.E. Iliffe, (Eds) Basin modeling : Practice and Progress, Geological Society, London, Special Publications, 141, 15-43.
- Hassan, A., K. Pohlmann, and J. Chapman, 2002, Modelling groundwater flow and transport of radionuclides at Amchitka Island's Underground Nuclear tests: Milrow, Long Shot and Cannikin, report submitted to Nevada Operations Office, National Nuclear Security Administration, U.S. Department of Energy.
- Rodi, W., R. L. Mackie, 2001, Nonlinear conjugate gradients algorithm for 2-D magnetotelluric inversion, Geophysics, 66, 174-187.
- United States Army Corps of Engineers, 1965, Project Long Shot, Amchitka Island, Alaska; geologic and hydrologic investigations (phase I) Prepared by U.S. Army Engineer District, Alaska and U.S. Geologic Survey, Anchorage.
- Wagner, A.M., D. Barnes, M.J. Unsworth and D. Kosson, 2006, Determining radionuclide seepage zones and groundwater travel times at Long Shot, in preparation for Journal of Hydrogeology.
- Wheatcraft, S.W., 1995, Sea water intrusion model of Amchitka Island, Alaska. Nevada Operations Office, U.S. Department of Energy, Report DOE/NV/10845-59.

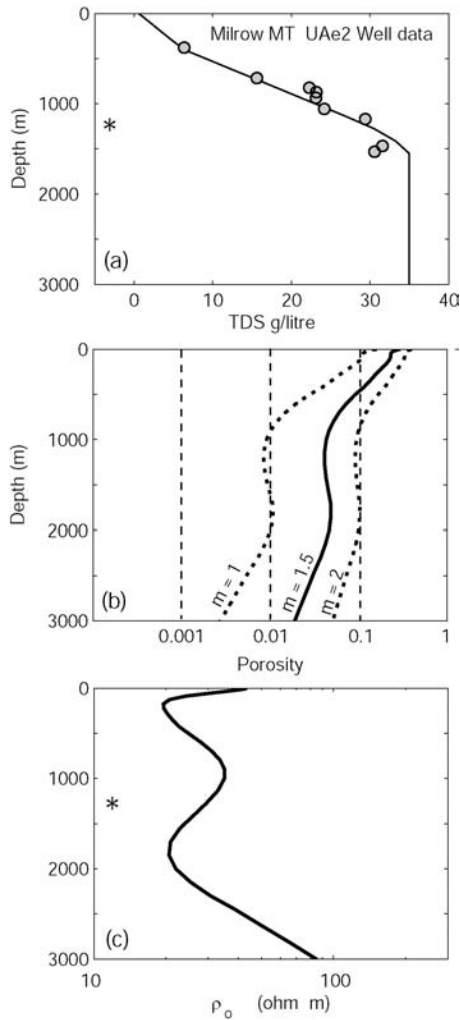


**Figure 3.** Hydrogeology for the Milrow explosion site. (a) Shows the salinity (TDS) at the nearby UAe-2 well (circles) and the line denotes a simplified form. The maximum value is 35 g/l equivalent to seawater. (b) Effective porosity required to give agreement between bulk resistivity and that determined by the MT data. Computation uses Archie's Law with exponents  $m=1$ , 1.5 and 2 (c) Resistivity from MT data inversion. The asterisk (\*) denotes the depth of the explosion.

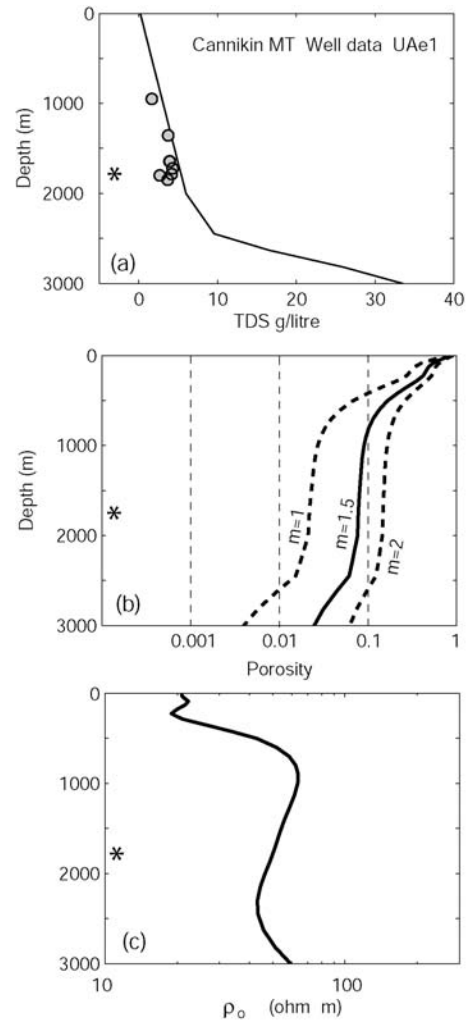


**Figure 4.** Hydrogeology for the Cannikin explosion site using salinity data from the coincident UAe-1 well. (a) Salinity in UAe-1 well. (b) Porosity values computed as in Figure 3. (c) Resistivity from MT data inversion. The asterisk (\*) denotes the depth of the explosion.